AD NUMBER

AD853678

LIMITATION CHANGES

TO:

Approved for public release; distribution is unlimited.

FROM:

Distribution authorized to U.S. Gov't. agencies and their contractors; Critical Technology; FEB 1969. Other requests shall be referred to Air Force Institute of Technology, AFIT-SE, Wright-Patterson, AFB, OH 45433. This document contains export-controlled technical data.

AUTHORITY

AFIT memo, 22 Jul 1971

AIR FORCE INSTITUTE OF TECHNOLOGY

AIR UNIVERSITY
UNITED STATES AIR FORCE

SCHOOL OF ENGINEERING

WRIGHT-PATTERSON AIR FORCE BASE, OHIO

A

PHOTOELECTRIC POSITION DETECTOR FOR SATELLITE TRACKING

THESIS

GSP/PH/69-11 Louis S. Macknik
1/Lt USAF

AFLC-WPAFB-JUN 69 34

BLANK PAGE

A PHOTOELECTRIC POSITION DETECTOR FOR SATELLITE TRACKING

THESIS

Presented to the Faculty of the School of Engineering of
the Air Force Institute of Technology
Air University
in Partial Fulfillment of the
Requirements for the Degree of
Master of Science

by

Louis S. Macknik, B.S.E.E.
1/ Lt USAF

Graduate Engineering Space Physics

February 1969

Preface

When the idea of designing a photoelectric satellite tracker was suggested to me as a thesis topic, I jumped at the opportunity to join together two of my greatest interests, electronics and astronomy. You might question the parallel between satellites and astronomy, but I considered the project to be a step in the right direction. The topic was a challenge because it encompassed a variety of subjects, including optics, mechanics, electronics, and ultimately an association with objects no longer of this world.

In this paper I have tried to show how known theory, method, and hardware were combined to yield the product, one unlike any other in existence, tailored to meet the needs of satellite tracking. The position detector was designed primarily for satellites, targets whose brightness is a function of many variables. The conditions and mechanisms which bring about the changes in satellite brightness have not been covered in this paper, for they are a complete study in themselves.

I am indebted to Dr. K.E. Kissell, Director of the General Physics Laboratory, whose experience, encouragement, and suggestions were indispensible to me. I am grateful, also, to R.C. Vanderburgh for his help on many nights of observation, for teaching me the techniques of tracking, and for the many profitable discussions of my problems.

L.S. Macknik

Contents

List of Figures

Abstract

A photoelectric position detector consisting of two photomultiplier tubes and an image splitter, and associated electronics, was built and evaluated as a satellite tracker. An automatic gain control utilizing negative feedback maintained the sum of the anode currents of the photomultiplier tubes constant under varying light flux levels, resulting in a large range compression. The difference of the anode currents was used to generate a signal proportional to the position error of the optical image of the target. The detector was tested in a servosystem on a 24-inch Cassegrain telescope, mounted on a 4-axis mount. Using stars and 51 transits of satellites, it was determined that the detector could track targets to within one radius of their optical image in the telescope, over a dynamic range of ten thousand in brightness. The lower limit for the detector was 4×10^{-11} lumens. Noise considerations and imbalance between the multiplier tubes resulted in the rejection of the detector as a photometer. However, the automatic gain control virtually eliminated any confusion of the detector by bright stars and variable brightness targets. Operation of the detector with the servosystem yielded certain modifications of the original detector to improve its performance.

I. Introduction

The purpose of this thesis is to describe the design of a photoelectric position detector and its experimental evaluation as a sensor for satellite tracking. The position detector is a device which can sense the location of an optical image within its entrance aperture. It was made to fill the need for an angular position sensor for the satellite tracker telescope maintained by the Aerospace Research Laboratories, WPAFB, Ohio. The telescope is used for photoelectric photometry of artificial earth satellites (Ref 9: 71-99).

Photoelectric photometry of earth satellites requires that small entrance apertures be used on photometers to limit the amount of sky background illumination. The smallest aperture that can be used is determined by the tracking capability of the telescope-observer combination. The ARL satellite tracker allows a skillful observer to track targets with angular velocities up to 3 degrees per second in a 120 arcsecond aperture. Tracking is accomplished by an angular rate control system on the tracking axis of the telescope and a position control on the crosstrack axis (perpendicular to the motion of the target). Errors inherent in the tracking technique require the observer to make manual corrections during a satellite transit (Ref 19). An angular position detector to correct for positioning errors in the tracking direction would improve efficiency in two ways. First, it would allow the observer more time for crosstrack corrections. Second, it would allow the use of a smaller entrance aperture on the photometer due to the increase in the tracking accuracy.

It was determined by the author that a suitable position detector must exhibit four basic characteristics. First, it must detect the location of an optical image in its own entrance aperture. Second, it must interpret the location of the image as an error signal in position with respect to the center of the aperture. The error signal must be of a form that can readily be used in a closed-loop position control system. Third, operation of the device must be independent of image brightness. Fourth, the detector must use analog (direct current or DC) methods. The first characteristic requires no explanation. The second is not unlike that found in many "star trackers" used on space vehicles and on astronomical telescopes. The third is more restrictive. While most star trackers are designed to operate on a fixed input light flux (which is determined by manually setting the gain), the desired detector must perform with incident fluxes over a dynamic range of 10^4 to 10^6 : 1 . Satellite brightness is a function of many factors. In general, satellites which are spherical or stabilized will not show large variations in the amount of sunlight they reflect. However, objects which are tumbling and/ or exhibit specular behavior usually produce large changes which may occur in a very short time. The detector must be capable of automatically sensing bright targets without saturating and dim targets without loss of position information. An example of the extremes which may be encountered is the Geos vehicle which carried xenon flash lamps. The change in brightness from the normal target brightness to the peak of a lamp flash was 6.5×10^4 in less than 2 milliseconds (Ref 9: 75). The fourth characteristic (analog operation) would allow the evaluation of

the detector as a photometer, thus providing brightness data as well as position information simultaneously.

A literature search revealed only one device which could meet more than the first two requirements. It was limited, however, by a dynamic range of 500:1 and it used AC techniques (Ref 15: 691-695). The existing photometer on the ARL telescope provided the starting point for the development of the position detector. That development will be described in the following order: theory of operation, experimental development, adaptation to a satellite tracker, and tests with space targets and results. The formal thesis will end with a short section on concluding remarks.

BLANK PAGE

II. Theory of Operation

To create a position detector which would have the four basic characteristics outlined above, a concept was developed which took full advantage of an existing device, one which exhibited the two most elusive characteristics of the four, independence from target intensity and DC operation. That device is the logarithmic response photometer used on the ARL telescope. In effect, two such photometers are combined to detect the position of an optical image by a comparison of the light levels transmitted to the photometers from a split image. A discussion of how the ARL photometer achieves independence from target brightness will be followed by a description of the logarithmic response position detector and its applicability to a position control system.

Logarithmic Response Photometer

The ARL photometer achieves DC operation over a wide range of target brightness (10^4 to 10^6 :1) through the use of a range compression technique first introduced by M. H. Sweet (Ref 18: 35-62). The range of operation is compressed by reducing the sensitivity of the detecting element, a photomultiplier tube, as the incident flux level increases.

A photomultiplier tube (PM) consists of a photoemissive cathode and an electron multiplier. The multiplier contains secondary-emissive electrodes (dynodes) and an anode. Photons, impinging on the cathode, produce photoelectrons which are attracted to the first dynode by an electrostatic field, thereby creating a "photocurrent", i_c . Upon striking the first dynode, the photoelectrons produce secondary-emission

electrons which are in turn attracted to the second dynode, and so on. The resulting current at the last element, the anode, is a much amplified version of the photocurrent. The process leads to the following equation(Ref 11: 226-229):

$$i_o = i_c k^n \tag{1}$$

where i_o is the anode current, k is the multiplication per dynode stage due to secondary emission, and n is the number of stages in the multiplier. The multiplication per stage, k, is a function of the voltage on the stage, E_d , and can be described as

$$k = KE_d^{\beta} \tag{2}$$

where K is a constant and β is a measure of the secondary-emission efficiency. The cathode photocurrent can also be expressed as

$$i_c = FS_c \tag{3}$$

where F is the incident light flux in lumens and S_c is the luminous sensitivity of the cathode in amperes per lumen. Eqs (1), (2), and (3) may be combined to obtain a new expression for the anode current:

$$i_o = FS_c K^n E_d^{n\beta} \tag{4}$$

In terms of overall PM performance, the anode current can be considered to be

$$i_o = FS \tag{5}$$

where S is the overall sensitivity of the PM tube in amperes per lumen. The overall sensitivity S then varies with the dynode voltage as

$$S = mE_d^{n\beta} \tag{6}$$

where m is the constant product $S_c K^n$. To achieve a wide operating

range the anode current must be maintained below one microampere in modern PM tubes to avoid fatigue effects (Ref 4: 423). From Eq (4) it is obvious that as F increases E_d may be decreased to keep the anode current i_o small. In particular, if i_o is to remain constant, then the product SF from Eq (5) must remain constant. The relationship between the sensitivity S and dynode voltage E_d can more easily be seen by taking the logarithm of both sides of Eq (6):

$$\text{Log } S = n\beta \text{ Log } E_d + \text{ Log } m \tag{7}$$

Although it is not apparent from Eq (7), M. H. Sweet has shown that as the number of stages n increases the relationship between Log S and E_d becomes increasingly more linear (Ref 18: 41). Since the product SF is constant for constant i_o, Eq (7) can be transformed into

$$\text{Log}F = -n\beta \text{ Log}E_d + \text{Log}c \tag{8}$$

where c is the constant ratio of i_o to m. For large n then, the change in Log F is linear with the change in E_d. Since this paper will later be concerned with space targets, it is convenient at this point to introduce the concept of stellar magnitude (a logarithmic scale used to describe the brightness of stars). The difference in stellar magnitude of two light sources is related to their respective fluxes as

$$p - q = -2.5\text{Log}\left[F_p / F_q \right] \tag{9}$$

where p and q are the stellar magnitudes of the two light sources, and F_p and F_q are their respective fluxes (Ref 1: 330). Since LogF is linear with E_d, the logarithm of the ratio of two fluxes will be proportional to a linear change in E_d. Hence, the relationship between the difference in stellar magnitudes and dynode voltage is linear if the anode current

is held constant and n is sufficiently large. For p otometry of space targets, this relationship provides a convenient means for measuring target brightness in stellar magnitudes. A portion of ' e dynode voltage may be sampled and recorded as a direct me asure of target brightness.

The foregoing discussion was intended to point out that a wide operating range could be obtained with a light-sensitive detector by capitalizing on its inherent characteristics. The photomultiplier tube is capable of high overall sensitivity , allowing the detection of small quantities of light. By reducing its sensitivity, much larger quantities of light may be measured without saturating the device. The sensitivity may be adjusted manually by changing the dynode voltage E_d . However, if one is to work with light sources which exhibit somewhat unpredict - able behavior, an automatic means for sensitivity adjustment is almost mandatory.

The ARL photometer employs circuitry which automatically sets the sensitivity of the PM according to target brightness. A simplified schematic diagram of that photometer is shown in Fig. 1 . Operation is that of a negative-feedback control system, with dynode voltage being varied to control the anode current of the PM. As the incident flux F increases, the anode current i_o will tend to increase according to Eq (5). The photometer is assumed to be at some sensitivity S_1 . As i_o increases, the grid-to-cathode voltage E_g on the 6AU5 control tube goes more negative by an amount $i_o R_L$, causing the 6AU5 to conduct less. The current I flowing through the control tube also flows through a voltage-divider resistance R which develops the dynode voltages for the PM; the total dynode voltage is IR . The decrease in I results in

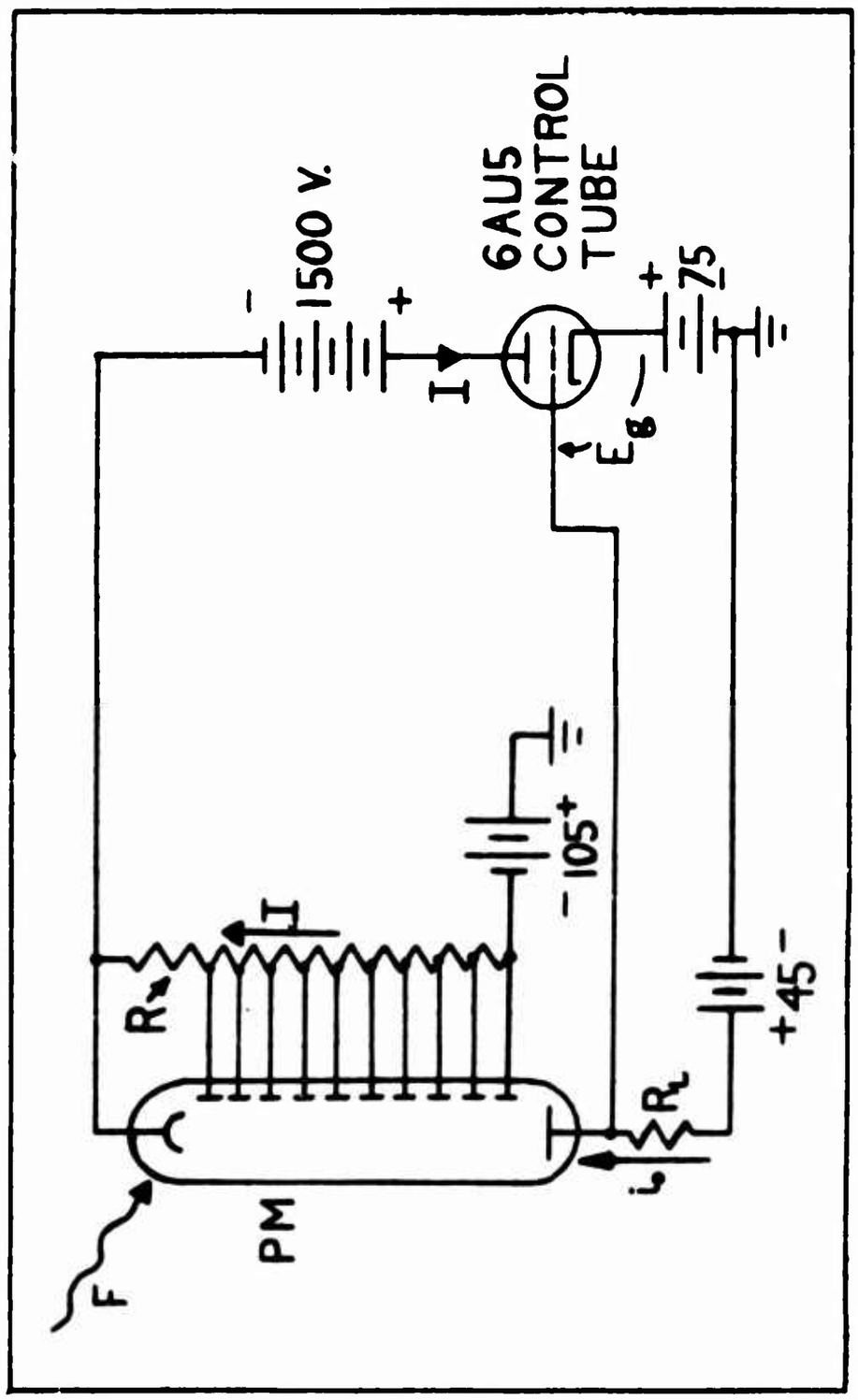

Fig. 1. Simplified Schematic Diagram of Logarithmic Photometer.

a decrease in dynode voltage. By Eq (6) then, the sensitivity of the PM decreases. The increase in anode current due to an increase in flux is therefore much smaller than would be the case with constant sensitivity. If the gain of the feedback loop were infinite, the anode current would remain constant. In practice, the anode current increases by approximately 0.1 microampere over the entire operating range of the photometer. The response time of the circuit is such that photometry of variable light sources with frequencies up to 5 kHz. is possible (Ref 9: 75). Not shown in Fig. 1 is the circuitry for sampling the total dynode voltage to provide an analog record of voltage which is nearly linear with stellar magnitude.

The useful range of the ARL photometer is limited at low flux levels by the "dark current" output of the PM tube and at high flux levels by the ability of the feedback loop to hold the anode current sensibly constant. The dark current consists of contributions to the total anode current from ohmic leakage, amplified thermionic emission and regenerative ionization (Ref 4: 24). Ohmic leakage produces most of the dark current at low dynode voltage. At medium voltages, the dark current is dominated by thermionic emission. At high voltages, an unstable condition can be encountered where large pulses of noise occur, probably due to secondary-emission of positive ions or photo-emission from excited gas, glass, or insulating material in the PM. Photomultiplier tubes are usually operated such that thermionic emission is the dominant source of dark current.

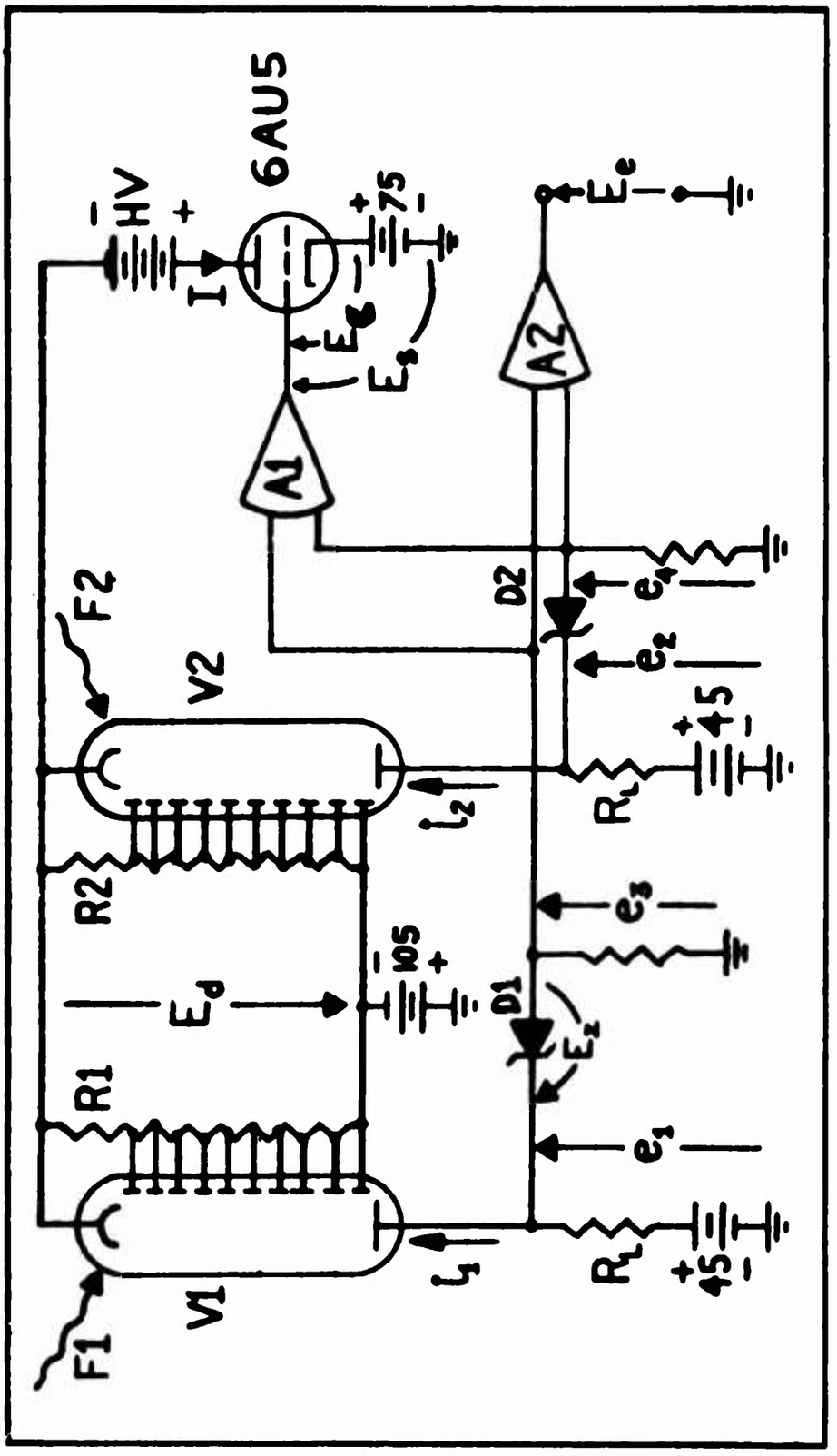

Fig. 2. Simplified Schematic Diagram of Logarithmic Position Detector.

Logarithmic Response Position Detector

The ARL photometer circuit was modified to enable detection of the position of the light source while maintaining the desirable DC operation and logarithmic response. The modification employed two PM tubes in a balanced-bridge configuration. Circuit parameters were adjusted so that a common negative-feedback loop could be used, with operating conditions identical to the original ARL photometer. Fig. 2 is a simplified schematic diagram of the position detector. Proper operation is based upon the following assumptions. It is assumed that the total flux incident on the PM's is given by

$$F = F_1 + F_2 \tag{10}$$

where F is the total flux, F_1 is the flux incident on V_1, and F_2 is the flux incident on V_2. It is not important at this point exactly how the flux becomes divided. Of several available methods, the author chose to use the principle of Fresnel's Biprism. It is assumed that the dynode voltage-divider resistances R_1 and R_2 are identical and equal to twice the resistance used in the ARL photometer. The 6AU5 control tube operates over the same range as before; that is, its plate current I and grid voltage E_g are the same as before. The most important assumption is that the two PM tubes are identical in every respect. With these assumptions, the negative-feedback and error signal generation will now be discussed.

Feedback. For the feedback loop to operate as in the ARL photometer, the grid voltage on the 6AU5 must vary in the same manner as

before. This can be shown to be true. Assume that the sensitivity of the detector is S_1 . Both PM's will have the same sensitivity since they are identical and share the same dynode voltage E_d . Referring to Fig. 2, e_1 and e_2 are defined as the output voltages from the PM tubes and are equal to

$$e_1 = 45 - i_1 R_L \tag{11}$$

and

$$e_2 = 45 - i_2 R_L \tag{12}$$

where i_1 and i_2 are the anode currents of the PM tubes and R_L is the load resistance in each PM anode circuit. Voltages e_3 and e_4 are generated by using zener diodes D_1 and D_2 to subtract a fixed voltage from e_1 and e_2 respectively. The voltage subtracted (equal to the zener voltage E_z) was chosen to be one-half of the output voltage (either e_1 or e_2) under zero flux conditions. Voltages e_3 and e_4 are then given by

$$e_3 = e_1 - E_z \tag{13}$$

and

$$e_4 = e_2 - E_z \tag{14}$$

E_z can be expressed in terms of Eq (11):

$$E_z = 0.5[45 - i_d R_L] \tag{15}$$

where i_d is the dark current of either tube, since the PM's are now assumed to be identical. The individual anode currents i_1 and i_2 can be considered to be composed of dark current i_d and current due to the incident flux, i_1' and i_2' respectively. This can be expressed as

$$i_1 = i_d + i_1' \tag{16}$$

and

$$i_2 = i_d + i_2' \tag{17}$$

Substituting Eqs (15), (16), and (17) into Eqs (13) and (14) and making use of Eqs (11) and (12) one obtains

$$e_3 = 22.5 - [0.5i_d + i_1']R_L \tag{18}$$

and

$$e_4 = 22.5 - [0.5i_d + i_2']R_L \tag{19}$$

The voltages e_3 and e_4 are applied to an operational amplifier A_1 which, with its associated circuitry, functions as a unity-gain, non-inverting summing stage (Ref 2: 60). Its output voltage E_s is the feedback voltage to the 6AU5 control tube. E_s is the sum of e_3 and e_4 and can be expressed as

$$E_s = 45 - [i_d + i_1' + i_2']R_L \tag{20}$$

Referring to Fig. 2, the control tube grid voltage can be written in terms of the PM anode currents as

$$E_g = -30 - [i_d + i_1' + i_2']R_L \tag{21}$$

If either V_1 or V_2 were used in the ARL photometer and a similar development carried out, the equation for E_g would be

$$E_g = -30 - [i_d + i_o']R_L \tag{22}$$

where i_o' is the anode current due to flux F. It is true that if the PM used in the ARL photometer is identical to the two used in the detector

then

$$i'_o = i'_1 + i'_2 \tag{23}$$

Eq (23) along with the assumption made in Eq (10) simply illustrate the fact that the relationship between incident flux and anode current is very linear (at a given sensitivity) (Ref 4: 423).

It has been shown that the negative-feedback loop operates under the same conditions as in the photometer; thus it can be concluded that the detector will have the same logarithmic characteristics as the photometer. It is also important to note that if Eqs (10) and (23) hold, then the motion of the image across the image-splitter will have no effect on the sensitivity so long as F is constant.

Error Signal Generation. While the sum of the anode currents does not vary with image motion, their difference does. This fact is used to generate the position error signal. Voltages e_3 and e_4 are applied also to operational amplifier A_2, which with its associated circuitry forms a unity-gain differential amplifier. Its output voltage E_e is defined as the Error Signal and is given arbitrarily by the difference of Eqs (18) and (19):

$$E_e = [i'_2 - i'_1]R_L \tag{24}$$

The difference formed here is arbitrary and remains so unless the Error Signal is used in a closed-loop. Then the physical positioning of the PM tubes will determine which difference is formed. From Eq(24) it is clear that the Error Signal will vary as an image moves across

the image-splitter, becoming negative, zero, or positive depending upon the relative magnitudes of the currents . The polarity of the Error Signal E_e is completely independent of the flux F. The maximum value of E_e will depend to some extent on the flux because the gain in the negative-feedback loop is finite in practice. As the flux F increases, the maximum absolute value of E_e will also increase.

Balance. It has been shown that for identical PM tubes the sensitivity of the detector is independent of image position and that the polarity of the Error Signal is not a function of target brightness. Unfortunately, identical PM tubes do not exist. The overall current amplification is equal to the average stage amplification raised to the nth power (n stages). Hence, a small variation in stage gain can yield a large change in overall gain. Great differences between tubes of the same type are not uncommon (Ref 14: 4). The difference usually is in the secondary-emission efficiency of the dynodes; that is, the value of β in Eq (2) differs from tube to tube (Ref 6: 89). Variations in gain can also be caused by differences in spectral response of the photocathodes, as the author discovered while trying to match the PM tubes he had selected.

In the negative-feedback path of the detector the sum of the anode currents must be sensibly constant at a given F as the image moves in the entrance aperture (as F_1 and F_2 vary). A difference in PM sensitivities would give rise to two effects under the conditions of a moving, constant brightness target. Considering Eq (24), if one of the currents increased faster than the other decreased with image

motion, the Error Signal would be distorted, indicating a smaller position error than actually existed. The other effect is that as the image moved, the dynode voltage would change since the sum of the currents would not be constant. If dynode voltage were being sampled as a measure of image brightness, the data would be modulated by the image motion. The other situation that could be affected by bridge imbalance is the condition where the image is stationary but varying in brightness. The amplitude of the Error Signal would follow the changes in brightness and could possibly change polarity if the PM tubes were sufficiently mismatched. On the other hand, the amplitude of the brightness change as indicated by the change in dynode voltage would be a function of the relative values of F_1 and F_2 ; that is, it would depend on the position of the image on the image-splitter. For the case where the image is moving and varying in brightness the situation would be very complex and little could be said about the position or brightness of the target.

It was anticipated that some balancing of PM characteristics would be required, which was, of course, the reason for using two separate voltage-dividers on the PM tubes. Three methods were considered for balancing. The first method was to attenuate the flux to the more sensitive tube, but this was disgarded as being inflexible. The second scheme was to lower the overall sensitivity of the more sensitive PM by dropping its overall dynode voltage lower than on the other tube. That technique is practical; indeed, it is the basis for the logarithmic response circuit. The third method was to alter the voltage to one dynode stage of the more sensitive PM, resulting in a loss

of gain due to the defocusing of the electron current stream within the tube (Ref 5: 527). The second and third methods were tried and the author found the defocusing technique to be superior in this application.

Application to A Control System

The feedback element of a position control system should exhibit the error signal depicted in Fig. 3 if it is a practical and linear element. The feedback element should not introduce noise into the

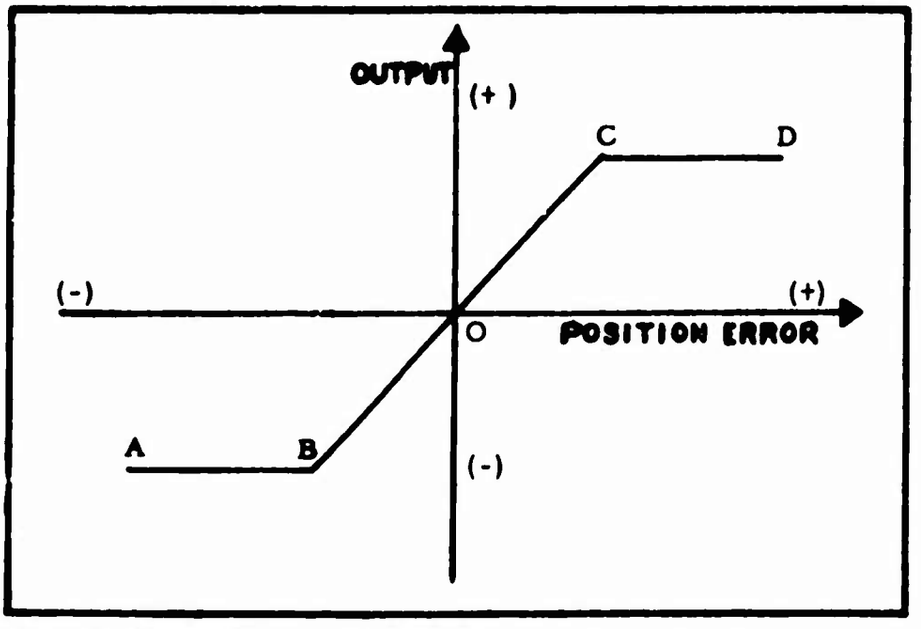

Fig. 3. Error Signal of a Practical Linear Feedback Element. Position information is available within the segment BOC where the output is linearly related to the position error. Segments AB and CD indicate that a practical device will saturate at some point. Within segments AB and CD, only the direction toward zero error is known by the sign of the output.

system, for noise will cause the controlling device to jitter about the desired position (Ref 13: 81). The noise produced by the detector was not negligible and had to be considered. Use of the photoelectric position detector in a closed-loop control system posed an interesting problem due to the nature of-its error signal.

Error Signal. The Error Signal from the detector does appear to be the same as in Fig. 3, except that a whole family of error signals results if one considers many values of incident flux F. This is true because E_e is not independent of target brightness. Fig. 4 shows Eq (24) plotted for several values of F. The resemblance to Fig. 3 is excellent ; however, one must be careful in interpreting Eq (24) as a true error signal, or feedback transfer function. What has not been

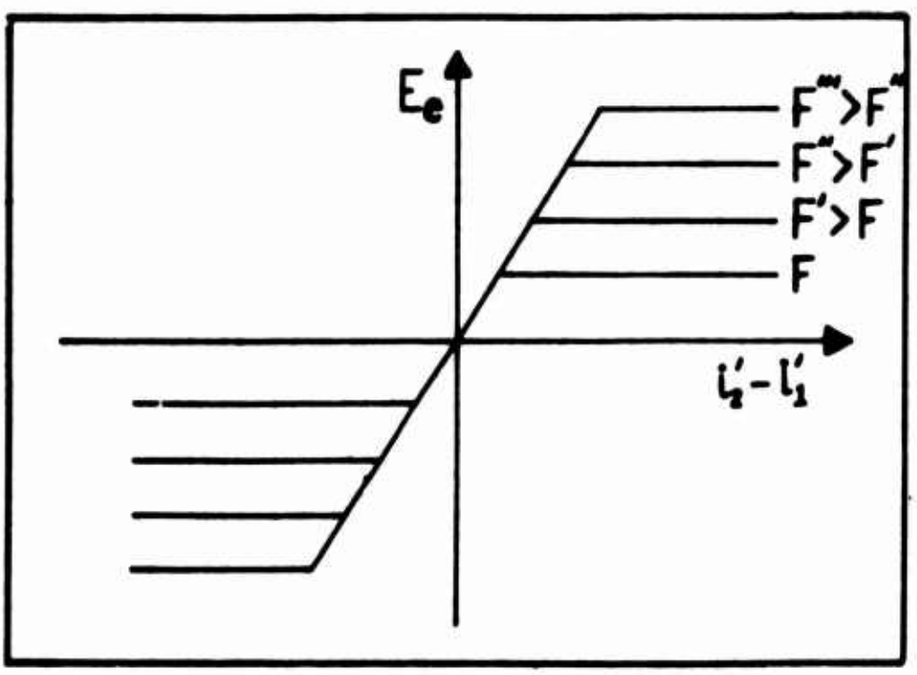

Fig. 4. Error Signal E_e as a Function of Current and Flux.

shown with Eq (24) is the variation of E_c with position. To obtain that information, one must know how the currents from the PM tubes vary with image motion. This in turn requires some knowledge of the image itself. Consider a circular image such as is formed with a point source and a circular lens (or telescope). For simplicity, only the bright disk in the center of the image is considered, and it is assumed to be uniformly bright. Some device which mechanizes Eq (10) is used to split the image to the two PM tubes. Fig. 5 shows the geometry involved.

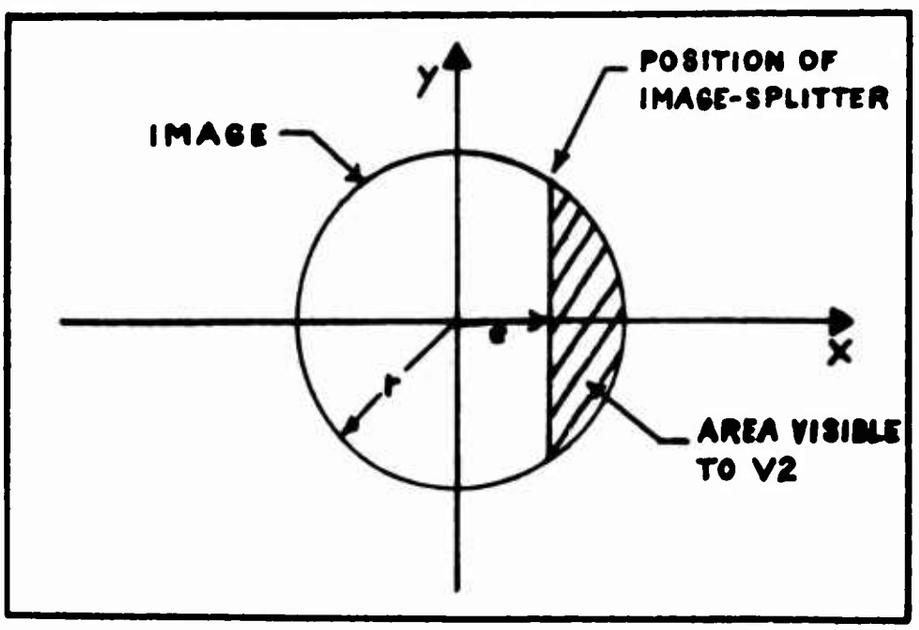

Fig. 5. Geometry of Image-splitting. A circular image of uniform brightness is assumed. The shaded area is "seen" by V_2 with the remaining area of the image visible to V_1. The radius of the image is r and the offset of the image center from the position of the image-splitter is e. The image-splitter is fixed in place, while the image and its "body-fixed" axes are free to translate in the x-direction.

The flux F_2 to PM V_2 is proportional to that part of the image area visible to V_2. Therefore the ratio of F_2 to F is the same as the ratio of the area visible to V_2 to the total area. These geometrical considerations lead to an expression for the ratio of F_2 to F :

$$\frac{F_2}{F} = \frac{\text{Cos}^{-1}(-P) + P\sqrt{1 - P^2}}{\pi} \tag{25}$$

where P is the negative of the ratio of e to r in Fig. 5 and is defined to be the position error. P is then zero when the center of the image is coincident with the position of the image-splitter. The ratio of F_1 to F is simply

$$\frac{F_1}{F} = 1 - \frac{F_2}{F} \tag{26}$$

from Eq (10). The form of the Error Signal as a function of position can be obtained by observing that

$$i_1' = SF_1 \tag{27}$$

and

$$i_2' = SF_2 \tag{28}$$

as suggested by Eq (5). Substituting Eqs (27) and (28) into Eq (24) gives

$$E_e = R_L S(F_2 - F_1) \tag{29}$$

which is equivalent to

$$E_e = R_L SF\left(\frac{F_2}{F} - \frac{F_1}{F}\right) \tag{30}$$

Eq (26) may now be substituted into Eq (30) to give

$$E_e = R_L SF\left[2\left(\frac{F_2}{F}\right) - 1\right] \tag{31}$$

Finally, the desired form is obtained using Eq (25) to introduce the

geometry of the image-splitting into Eq (31):

$$E_e = R_L SF\left[\frac{2\mathrm{Cos}^{-1}(-P) + 2P\sqrt{1-P^2}}{\pi} - 1 \right] \quad (32)$$

The bracketed portion is simply a geometric factor describing the modulation of E_e by the image motion. The product SF is the total anode current flowing due to a total flux F incident on the detector at a sensitivity S. The term $R_L SF$ is then the maximum value of E_e in volts. It is recognized that Eq (32) is valid only for those values of P such that $-1 \leqq P \leqq 1$, but that is enough to completely specify E_e since E_e is not a function of position beyond those limits. There is no variation in the anode currents when the image is not being split, assuming constant F. The product SF is not constant since the gain of the feedback loop is finite. Therefore, E_e will increase with an increase in F. Fig. 6 was plotted from Eq (32) with E_e in relative units versus position error for various values of F. Position data is

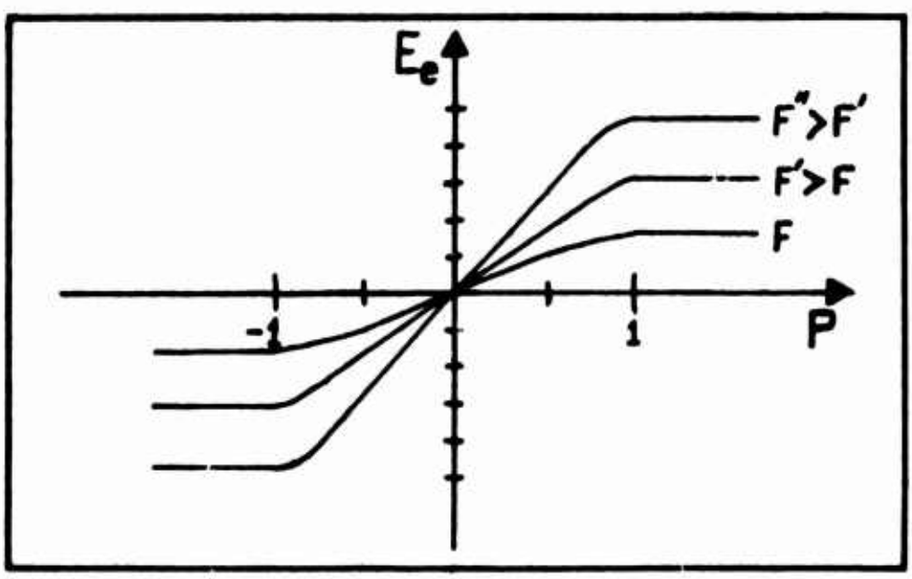

Fig. 6. Error Signal as a Function of Position Error and Flux. Both maximum value and slope of E_e vary with flux.

available only when P lies between -1 and 1. Otherwise, only the direction towards zero position error can be inferred. From Fig. 6 it is obvious that the slope of the Error Signal is a function of target brightness. This result can create a problem when the detector is used in a closed-loop system. The variable slope will produce a variable closed-loop gain; that is, the number of volts per unit angle of error will vary. If the loop gain is initially set to provide optimum control with the dimmest targets, the gain may rise sufficiently on bright targets to render the system unstable. If the loop gain is set to provide stable operation on the brightest targets, then the loop gain may drop too low on dim targets to allow satisfactory control. This behavior was taken into account when the author designed the feedback compensation in the optical feedback path of the position control system described in Chapter IV.

Noise. The Error Signal from the detector is generated by the differencing of voltages which are proportional to the anode currents of the PM tubes. Noise from the PM tubes is not cancelled in this process since the noise from two sources is governed by

$$N^2 = N_1^2 + N_2^2 \tag{33}$$

where N is the total r.m.s. noise voltage, and N_1 and N_2 are the r.m.s. noise voltages from the PM tubes V_1 and V_2 respectively. The addition of two sources of noise is independent of any phase relationships (Ref 16: 216). The noise current from a photomultiplier tube can be given by Eq (34) if the PM tube is operated under such

conditions that thermionic emission is the dominant source of noise:

$$I_n^2 = 2qBGi \qquad (34)$$

where I_n is the noise current, q is the electron charge, B is the bandwidth of the system, G is the current amplification and i is the total anode current including dark current and signal current (Ref 15:694). The noise current due to two PM tubes can be found by replacing i in Eq (34) by the sum of the anode currents of the two tubes. It is then predicted that the noise associated with the detector will vary as the square-root of the sensitivity. Since sensitivity varies inversely with target brightness, the noise will vary inversely with the square-root of target brightness. Hence, the noise will be greatest when attempting to detect dim targets. Decreasing the bandwidth B of the system in which the detector operates will improve the ability to detect dim targets.

III. Experimental Development

A prototype position detector was built by the author to apply the above theory to hardware. Construction was guided by the knowledge that the detector would ultimately be tested in a closed-loop control system for satellite tracking. The following is a discussion of the prototype development and laboratory tests performed on it.

Position Detector Prototype

Construction of the detector involved selecting two suitable PM tubes, designing the circuitry, and assembling the parts in a manner dictated by the optics involved.

Photomultiplier Selection. The PM tube chosen was the RCA Developmental C-70038D, a 10-stage, dormer-window type designed for use in star-tracking guidance systems. It is especially suited for applications involving little contrast (high background illumination). Relative sensitivity measurements were made on three available tubes to determine which two of the three were more closely matched. The relative sensitivities of the tubes, as functions of cathode-to-dynode 10 voltage, are shown in Fig. 7. The voltage between dynode 10 and the anode was held constant at 150 volts to simulate the operating conditions of the detector circuit. The tubes chosen, identified by serial number in Fig. 7, were C11677 and C07182, although tests were made using C11677 and Z07686 as the "matched pair". The sensitivity curves were obtained by varying the incident light to each tube with neutral density filters and adjusting the voltage so that the anode current was

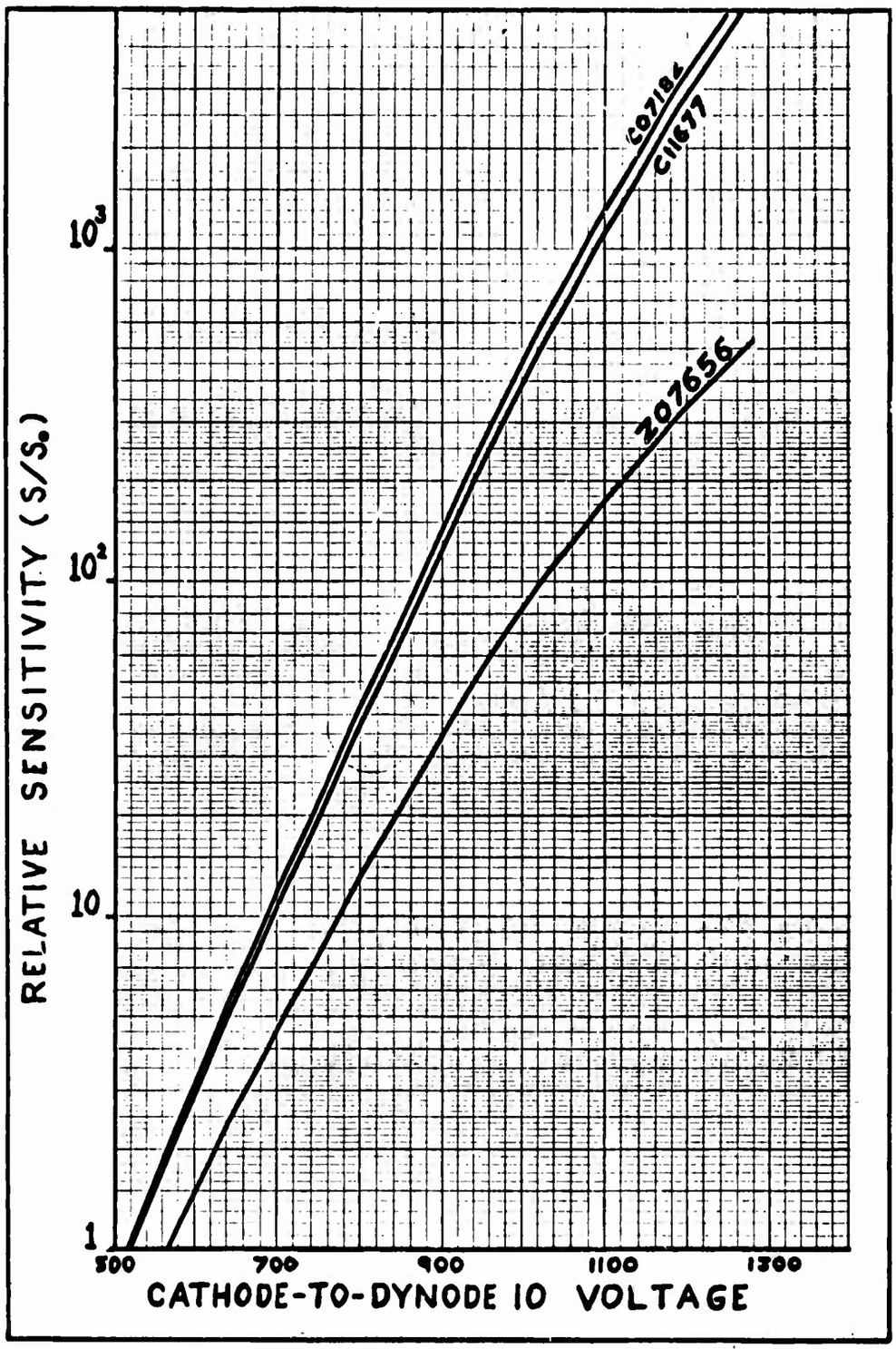

Fig. 7. Relative Sensitivities of Three C-70038D Multiplier Tubes. Each is identified by its own serial number. The voltage between the anode and dynode 10 was fixed at 150 volts.

constant at 10 nano-amperes.

Circuitry. A complete schematic diagram of the detector is shown in Fig. 8. Physically, the circuitry was divided into two parts: the main chassis and the detector head. The main chassis contained the 6AU5 control tube, OB2 and OA3 gaseous regulators to develop the -105 and + 75 voltage levels, two voltage-dividers to provide the + 45 volts to the PM load resistors, and a voltage-divider and cathode-follower (12AT7) to sample the dynode voltage for brightness measurements. The high voltage and low voltage power supplies were commercial units external to the main chassis. The detector head contained the PM tubes, their dynode voltage-divider resistors and load resistors, two cathode-followers (12AT7's) , and the optics for image-splitting. The cathode-followers in the detector head were used only for impedance-matching between the high impedance of the PM anodes and the low impedance of coaxial cables used for connection of the head to the operational amplifiers A_1 and A_2 . Insertion of a cathode-follower between each PM and the operational amplifiers did not disrupt the theory of operation because the output voltage from a cathode-follower is for all practical purposes the same as the input voltage; the cathode voltage follows the grid voltage very closely with a voltage gain of essentially one (Ref 12:192-196). The operational amplifiers were integral parts of a plug-in unit to a Tektronix oscilloscope. This allowed the inputs and outputs of the operational amplifiers to be monitored visually. A variable negative bias was provided for the 10th stage of V_2 to allow balancing by defocusing the

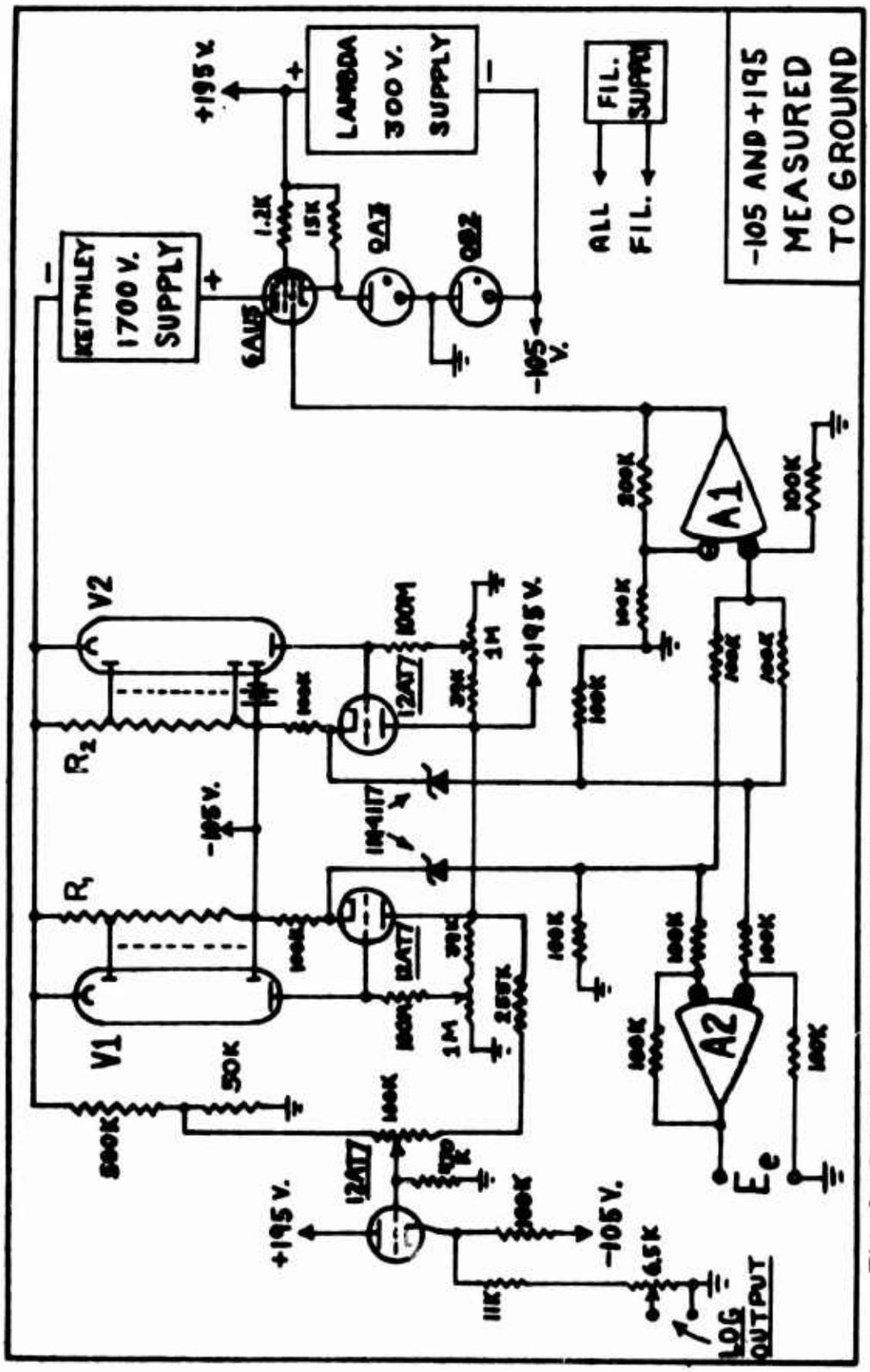

Fig. 8. Complete Schematic Diagram of Logarithmic Response Position Detector.

electron stream in the more sensitive tube.

Optical Arrangement. Fig. 9 shows a pictorial diagram of the method used for splitting the image. If an image is focused in the plane of the aperture, the prism will refract the light into two beams. The beams appear to originate at two virtual sources (images) as with a Fresnel biprism (Ref 7: 239-241). The brightness of the two virtual sources is dependent upon the position of the real image with respect to the edge of the prism. Eq (10) was mechanized in this manner. The prism may be used with the light entering from the flat side, but there is a limit on the apex angle in that mode, a limit which does not occur with the prism used as shown in Fig. 9. The author at first tried a

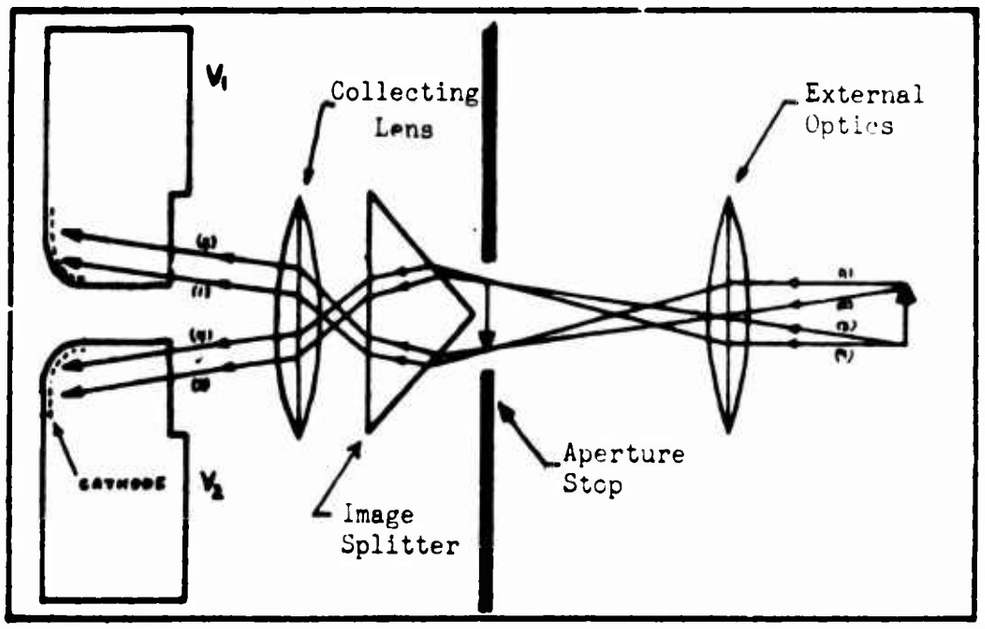

Fig. 9. Pictorial Diagram of Detector Optical Assembly.

Fresnel biprism; the angle of separation of the two beams was too small. A 90° prism was then tried. Splitting of the image did not occur when the light entered the prism from the flat face, but the image was split when the prism was used as in Fig. 9. The author found that total

internal reflection would occur for apex angles less than about 98°, when the light entered the flat face. A prism which could be used in either mode was obtained by suitably cutting a pentaprism, thereby yielding the prism in Fig. 9 with an angle of 112.5°. The separation angle is about 38° in this case. A lens was used to collect the two beams and direct them to the photocathodes of the PM tubes. The lens also imaged the aperture of the original light source with the result that as the image moved in the detector entrance aperture, the new images on the cathodes remained stationary but varied in brightness. The movement of the images on the cathodes is not desirable since the sensitivity of the photocathode is not uniform across its area. The detector aperture was made square, 7 mm. on a side. Fig. 10 is a photograph showing the detector head prototype with power connections, signal connections, and the square aperture in a cylindrical cover.

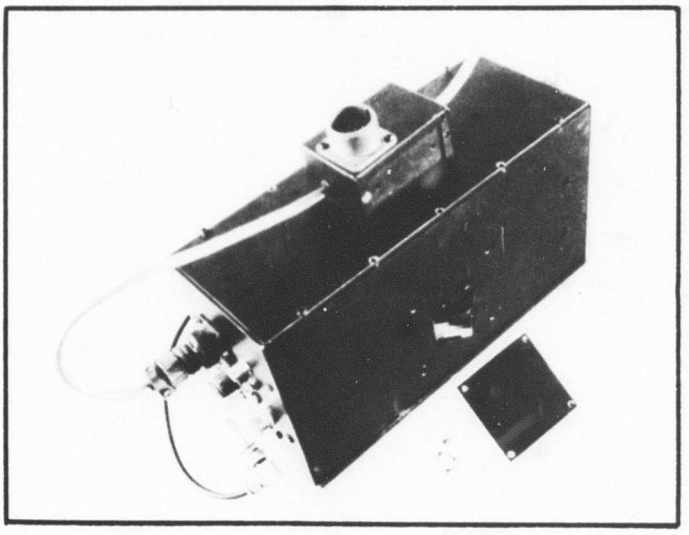

Fig. 10. Detector Head Prototype.

Laboratory Tests

Tests were conducted with the detector in the laboratory, using a light source mounted on a micrometer slide which could be moved at right angles to the optical axis of the detector. The light source had a 0.6 mm. circular aperture. An f-16 lens was used to focus an image of the source in the detector entrance aperture, producing an image at the prism of 0.1 mm. diameter. The f-16 lens was used to simulate the f-16 Cassegrain telescope used for satellite tracking. The scale factor in the focal plane of the telescope is 20.8 seconds of arc per mm.; a 0.1 mm. image therefore simulated a point source image of 2 arc-seconds diameter. Dr. K. E. Kissell, Director of the General Physics Laboratory of ARL, had pointed out to the author that 2 arc-seconds was a reasonable size for images of point sources in the telescope. Neutral density filters were used to vary the light to the detector. As the image was moved across the prism, the Error Signal and image brightness (dynode voltage) were recorded, for each value of incident flux.

Balance. It was mentioned under Circuitry that a variable bias was applied to dynode 10 of V_2 to effect balancing of PM characteristics. Hariharan and Bhalla used the technique to achieve balance between two PM tubes in a bridge circuit for the measurement of small changes in absorption (Ref 6: 89-90). The bias effectively increases the negative-feedback to V_2. Since the bias is fixed for normal operation, one can determine that it has more effect when the dynode voltage is small than when it is large. The range of gain over

which the tubes can be matched depends upon the degree of imbalance that can be tolerated. The bias in the detector was set to a value at which the balance was best for flux on the order of 10^{-7} lumens, which approximates a 2nd magnitude star in a 24 inch aperture telescope. The dimmest star which may be seen with excellent eyesight is of 6th magnitude. Balance was monitored by observing the brightness of the light source as indicated by the dynode voltage (at the Log Output in Fig. 8). Any imbalance caused a variation in dynode voltage as the image crossed from one side of the prism to the other. Another scheme for balancing was tried. It involved inserting a non-linear resistance in series with the high voltage lead to V_2 . This method could not provide the degree of balance obtained with the defocusing method. In addition, it suffered the disadvantage of being at potentials above 1000 volts and required special precautions to work. Fig. 11 shows Log Output voltage versus position error for several values of incident flux with no bias applied to V_2. In Fig. 12, 80 volts

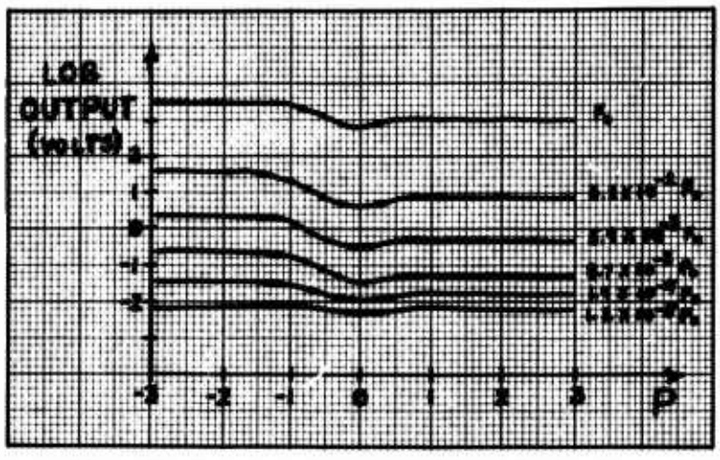

Fig. 11. Brightness measurement of a constant intensity source moving across the prism. The effect of bridge imbalance is apparent. Loss of light near zero error is caused by scattering off the edge of the prism. No bias applied.

bias has been applied. Note in Fig. 12 that the range over which the PM tubes are reasonably matched has increased, and that V_2 has actually become less sensitive than V_1 for high fluxes. That was the result of the bias being more effective at low dynode voltages.

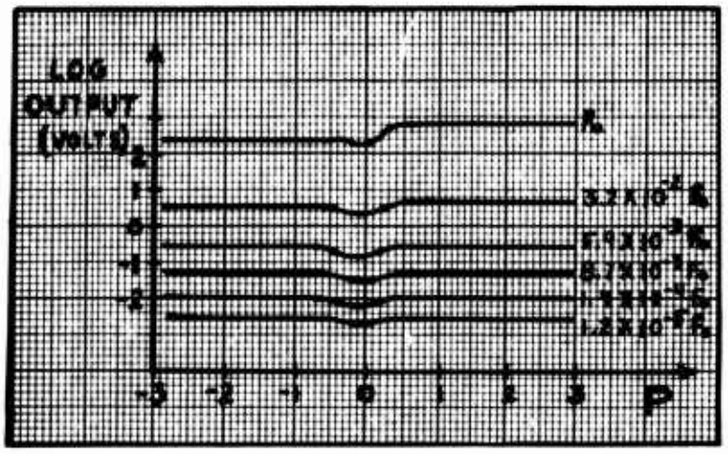

Fig. 12. Brightness measurement with 80 volts bias applied to the more sensitive PM tube.

Error Signal. The Error Signal was monitored simultaneously with the Log Output of the detector. The effects of bridge imbalance were readily detectable. The dependence of the Error Signal upon image brightness was also apparent since both maximum value and slope varied with incident flux levels. The point at which the image was exactly centered on the prism was found by noting the decrease in dynode voltage, evident in Figs. 11 and 12. The edge of the prism, with its non-zero width, scattered a certain portion of the light, giving rise to an apparent (but false) decrease in source brightness The Error Signal with no bias applied to V_2 is shown in Fig. 13 as a function of position error. The abscissa is in terms of -P as a

consequence of the author's test set-up and it was desirable to have the Error Signal in the same form as in Fig. 6. Fig. 14 shows the Error Signal with 80 volts bias applied to V_2. The application of 80

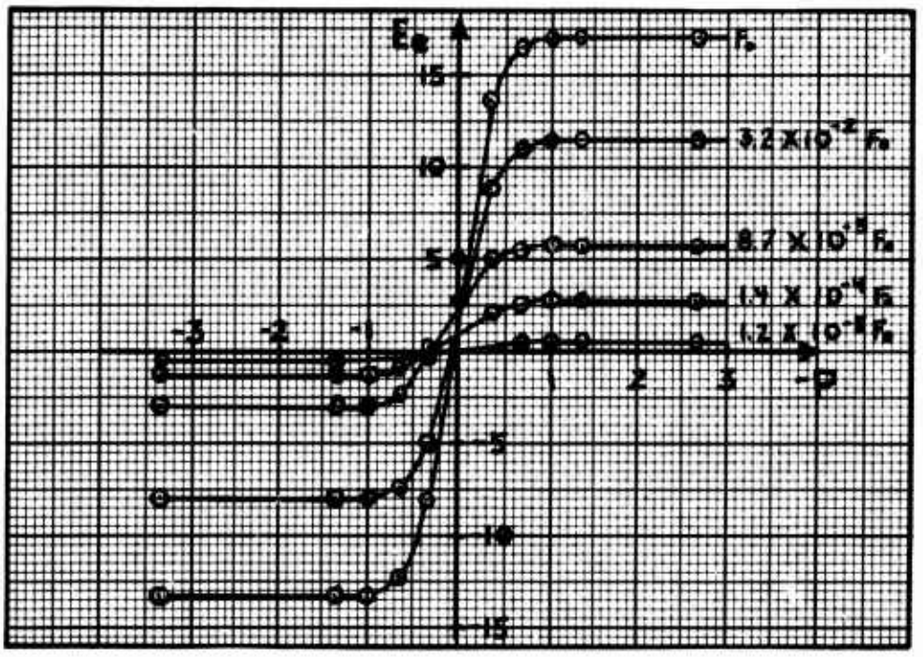

Fig.13. Measured Error Signal Vs. Position Error. No bias.

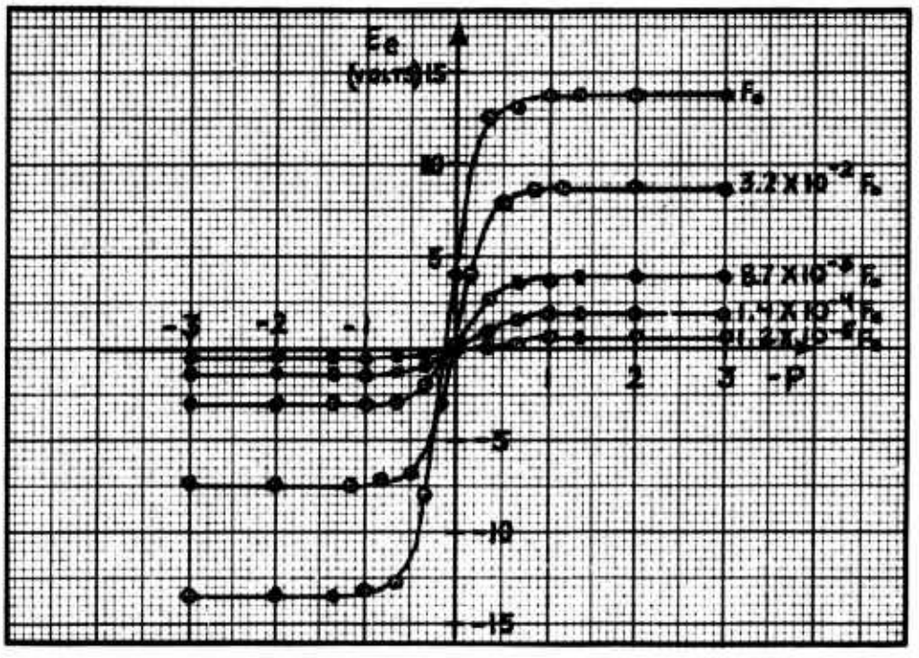

Fig.14. Measured Error Signal Vs. Position Error. 80 v. bias.

volts bias improved the symmetry about both axes. The range of flux over which the Error Signal became zero near the origin was increased. Note that, as in the brightness records, the direction of imbalance is opposite to that occurring without the bias applied. The point where P equalled zero could be determined to within ± 0.1 image radius. Dynode voltage was monitored visually on a galvanometer oscillograph and aurally with a tone which was frequency modulated by the dynode voltage. The change in dynode voltage which gave rise to the dips in the curves of Figs. 11 and 12 was easily detectable by this method.

Noise. No noticable variation in the noise level from the detector was observed during the laboratory experiments. It was concluded that the test equipment and the stages following the PM tubes were adding a sufficient amount of noise to mask any variations due to changes in gain of the detector. This was not the case in later tests with space targets. One of the PM tubes later became very noisy . Scintillation of targets due to atmospherics also contributed a noise component in those later tests.

IV. Adaptation to A Satellite Tracker

The performance of the detector as an optical sensor for a satellite tracker servosystem was evaluated by mating the detector to the 24 inch ARL telescope. For a proper evaluation, acceptable performance had to be defined. The author chose to use the ARL photometer as the main reference and defined tracking as being successful if the detector, feeding position information to the servo-system, could maintain a target within the photometer's entrance aperture.

Mating the detector to the telescope involved mounting the detector head at the Cassegrain focus, processing the Error Signal for use by the control system, and installing suitable instrumentation to monitor the detector's performance.

Mounting

The detector head was mounted so that its aperture could be aligned with the photometer aperture. A beamsplitter was used to provide an image to both the detector and the photometer. The beam-splitter, a partially-silvered mirror, transmitted 7.7% of the light to the photometer and reflected 26% to the detector. The aperture of the detector represented a square with sides of 146 arc-seconds in the telescope's focal plane. The detector was oriented so that errors in position about the tracking axis could be detected. The main chassis, power supplies, and operational amplifiers were located in another building approximately 75 feet from the telescope. Fig. 15 is a photo-graph of the ARL telescope. Fig. 16 shows the detector head mounted

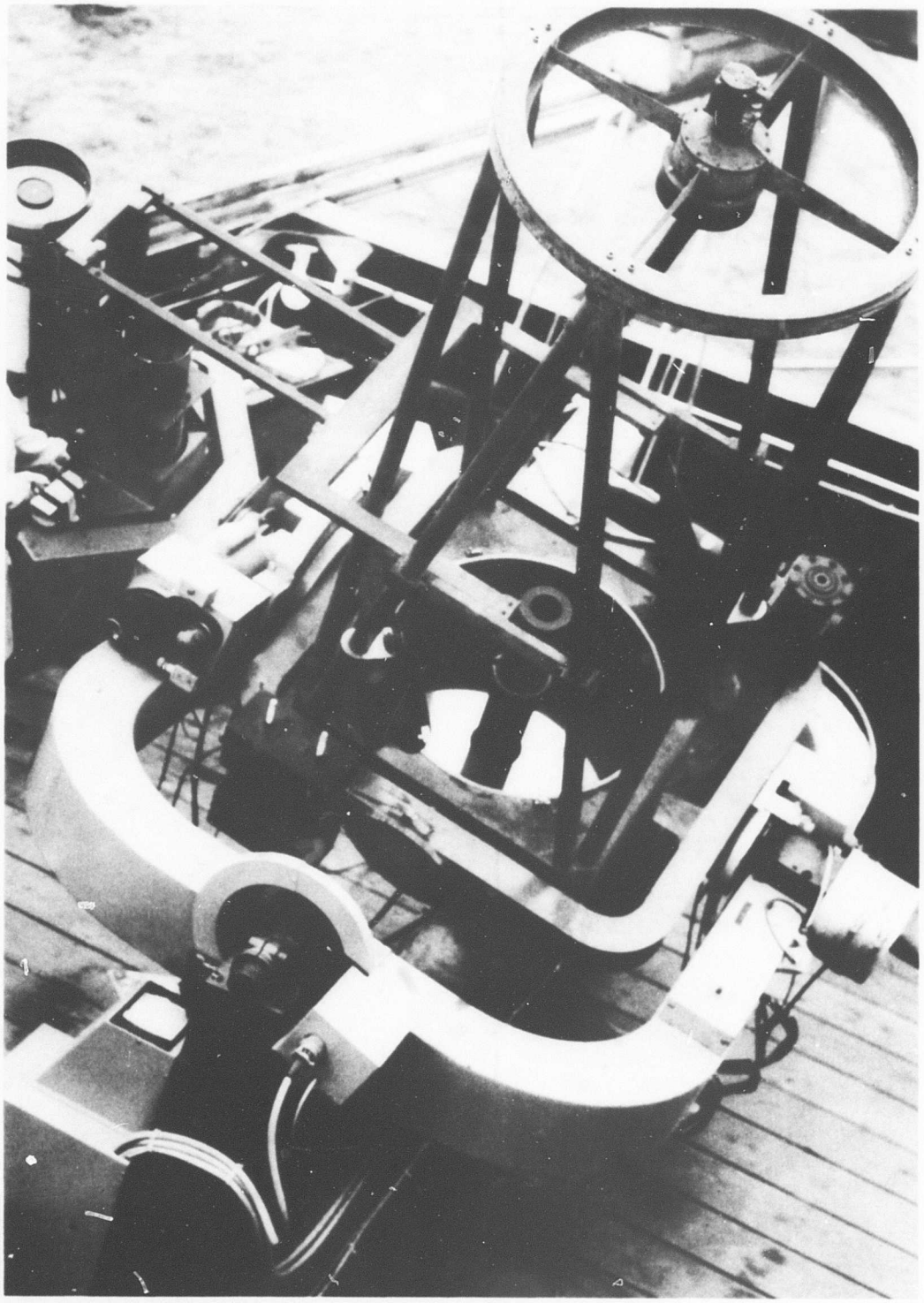

Fig.15. ARL 4-Axis Telescope .

on the telescope. The detector head is on the left; the enclosure in the center houses the beam-splitter. The ARL photometer is on the right.

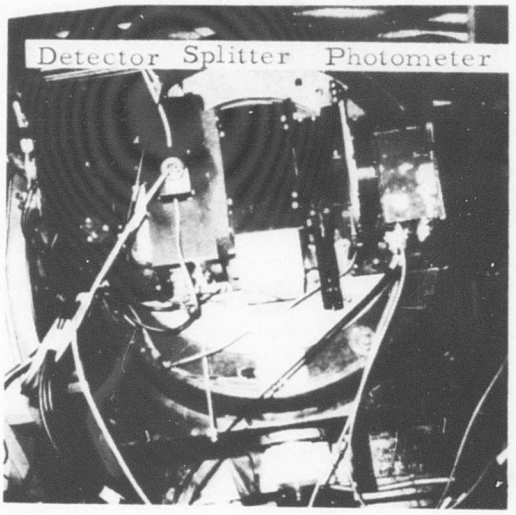

Fig. 16. Detector Head On the Telescope.

Error Signal Processing

The control system of the telescope normally provides an open-loop angular rate control on the tracking axis. The addition of the detector provides a closed-loop position control. Such a system is of second order, so much attention had to be given to damping of oscillations and removal of positioning errors. A tachometer was already incorporated in the rate control loop for damping (Ref 10: 177). The author chose to use proportional plus integral control to remove the steady-state position errors, as suggested by Kennedy, designer of the servosystem (Ref 8: 30). The Error Signal was processed through two phase-lag amplifiers which closely approximate integrators. They

were constructed with operational amplifiers and provided a very convenient means for adjusting the loop gain and compensation quickly (Ref 2: 67).

A great deal of experimenting was required to obtain the proper compensation. Integral, or lag, compensation does reduce steady-state positioning errors, but it also reduces the damping (Ref 10:181). This fact, along with the nature of the Error Signal, led to a system which was initially unstable. To compensate for the variable slope of the Error Signal, the voltage E_e was fed through a double-diode limiter as shown in Fig. 17. The output of the limiter is the same as the input until the voltage across the diodes reaches the junction potential of the diodes. One of the diodes will then begin to conduct; which one conducts will depend upon the polarity of the input voltage. With one diode in a conducting state, a voltage-divider is formed by the series resistor and the internal resistance of the diode. For the silicon diodes used, the junction potential was 0.6 volts; the internal resistance was 500 Ohms (Ref 17: 475). The stages of compensation that provided the best tracking can be described as a low-pass filter with an upper cut-off frequency of 0.08 Hz. and a DC gain of 5×10^{-3}. The tests that were performed to arrive at the required compensation are described in Chapter V.

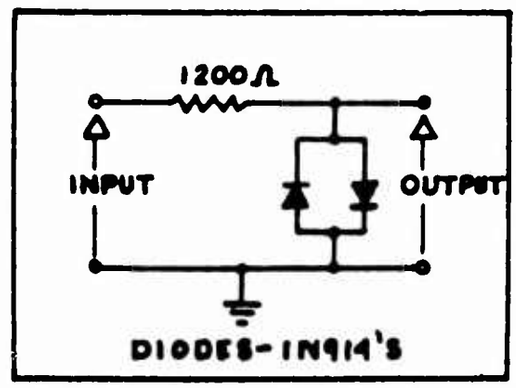

Fig. 17. Double-diode Limiter.

Instrumentation

The performance of the detector was monitored in two ways. First, it was necessary for the author to visually acquire and observe the targets with a guiding telescope to provide position corrections in the crosstrack direction. Qualitative measurements of the performance were made in that way. An audio tone modulated in frequency by the output of the photometer indicated when the targets were within the photometer's entrance aperture. Second, several quantities were measured in analog form on a seven channel FM tape recorder and on a galvanometer oscillograph simultaneously. The modified Error Signal (at the output of the limiter) was recorded in one channel. The Log Output of the detector, the Log Output of the photometer, and timing signals from a crystal clock and radio station WWV occupied other channels. One channel was used to record remarks from a microphone at the telescope. All recording equipment was housed in the equipment building and operated remotely. The galvanometer oscillograph provided immediate indications of the operation of the detector. The data recorded on magnetic tape could be played back at any time with almost any desired time compression or expansion for the analysis of the data.

Fig. 18 is a photograph of the equipment as it was housed in the equipment building. The electronics for the detector are on the left, including the main chassis, the operational amplifiers (and oscilloscope), and the power supplies. The FM tape recorder and timing equipment are in the center. The photometer electronics and the galvanometer oscillograph are in the rack on the right.

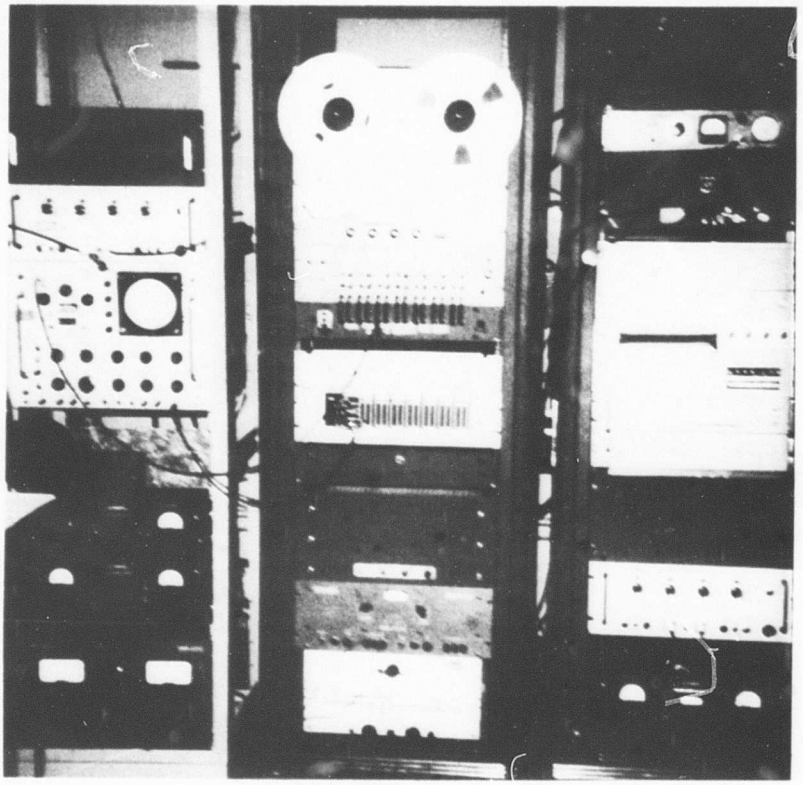

Fig. 18. Electronics Racks in Equipment Building. The detector main chassis, operational amplifiers, and power supplies are on the left. The FM tape recorder and timing equipment are in the center. The photometer and oscillograph are in the righthand rack. Operation was controlled remotely from the telescope.

V. Tests With Space Targets and Results

Experiments were conducted using both stars and earth satellites as targets. Stars provided constant point sources with which the author was able to optimize the characteristics of the position control system. They were also used to evaluate the detector as a photometer. Satellite tracking was the final step in the evaluation of the detector prototype. A discussion of the tests and results follows.

Tests

Tests with the detector mounted on the telescope were conducted over a three month period. Stars were used to provide information on the static characteristics of the detector-telescope combination. The dynamic behavior was studied using satellites.

Stars. Stars were used in two different experiments. The first was what the author called a "drift test". The telescope was configured in an equatorial mode without drive to the tracking (polar) axis and without the position control loop activated. Chosen stars were then drifted through the aperture of the detector, taking advantage of their diurnal motion. Stars were chosen from the G Class of spectral types so that the analysis of balance and error signal would be applicable to satellites illuminated by our Class G sun (Ref 1: 327-329). The balance and error signal obtained in that way were compared to the balance and error signal measured in the laboratory. Two combinations of PM tubes were tried, as mentioned on page 24. The second kind of experiment was identical to the first with the exception that the position control

loop was closed. Under that condition, the detector would maintain an image in the center of the aperture, causing the telescope to track at the star's diurnal rate. From the second experiment, the author gained information about the tracking errors and operating range of the system. The elements of lag compensation were adjusted during this phase to minimize the tracking errors.

Satellites. The experiments with stars provided the steady-state behavior (constant intensity sources). The dynamic characteristics were obtained by tracking 28 different satellites for a total of 51 passes. The targets were acquired with the system in the Aided-Rate mode; that is, the position control loop was open and an analog computer was generating an angular rate command to approximate the angular rate of the satellite. Once acquired, the position loop was closed and the target was tracked in the AUTO mode. The detector then provided the position information to "correct" the errors in the rate command from the computer. Those errors were due primarily to the approximations made in obtaining the angular rate equation which the analog computer mechanized (Ref 8: 4).

Results

The data taken with the stars and satellites were combined to describe the behavior of the detector as a sensor for the ARL satellite tracker. The behavior can best be explained by considering the following categories: operating range, tracking error, balance, and erroneous target rejection.

Operating Range. The compensation specified previously provided satisfactory tracking of targets from 9th magnitude to -1 magnitude. As brightness increases, stellar magnitude goes more negative; a 6th magnitude star is the dimmest that may be seen with excellent unaided eyesight on a clear night. The narrow bandwidth of the compensation (0.08 Hz.) would indicate that the error signal obtained from a 9th magnitude star was very nearly the same amplitude as the noise from the detector, or alternately that a long integration time was needed to pick the weak signal out of the noise. That was indeed the case during the three month period of tests with the telescope. The dark current of PM tube C11677 had greatly increased and was very erratic in nature. The author concluded that the tube was defective to the extent that regenerative ionization was occurring at normal operating voltages. The excess noise was tolerated, however, for reasons explained under the section entitled Balance. The narrow bandwidth of the system did reduce the transient response, but this turned out to be an asset when the problem of erroneous target rejection was considered. The observed fact that the system could not track below 9th magnitude is suggested also by the signal-to-noise ratio of the detector; that is, the ratio of the amplitude of the error signal to the amplitude of the noise in the error signal. The signal-to-noise ratio is defined as

$$\frac{S}{N} = \frac{E_e^2}{V} \qquad (35)$$

where S/ N is signal-to-noise ratio, E_e is the Error Signal, and V is the

mean-squared noise voltage (Ref 16: 226). It should be apparent that the S/ N will vary, not only with target brightness, but also with the target position on the image-splitter. For a given brightness, there will be a fixed amount of noise. As the image moves in the aperture, E_e will go to zero as position error approaches zero; therefore the S/ N will be zero at P= 0. With increasingly brighter targets, the noise from the detector decreases at the same time that E_e increases. Hence, there is the unfortunate situation that the S/ N is poorest with the dimmest targets. The concern at this point is with the dimmest target that will produce any discernible error signal at all, so the variation in S/ N with image position in the aperture will not be considered. With this reasoning, the signal-to-noise ratio as a function of stellar magnitude was plotted in Fig. 19. The Error Signal was taken

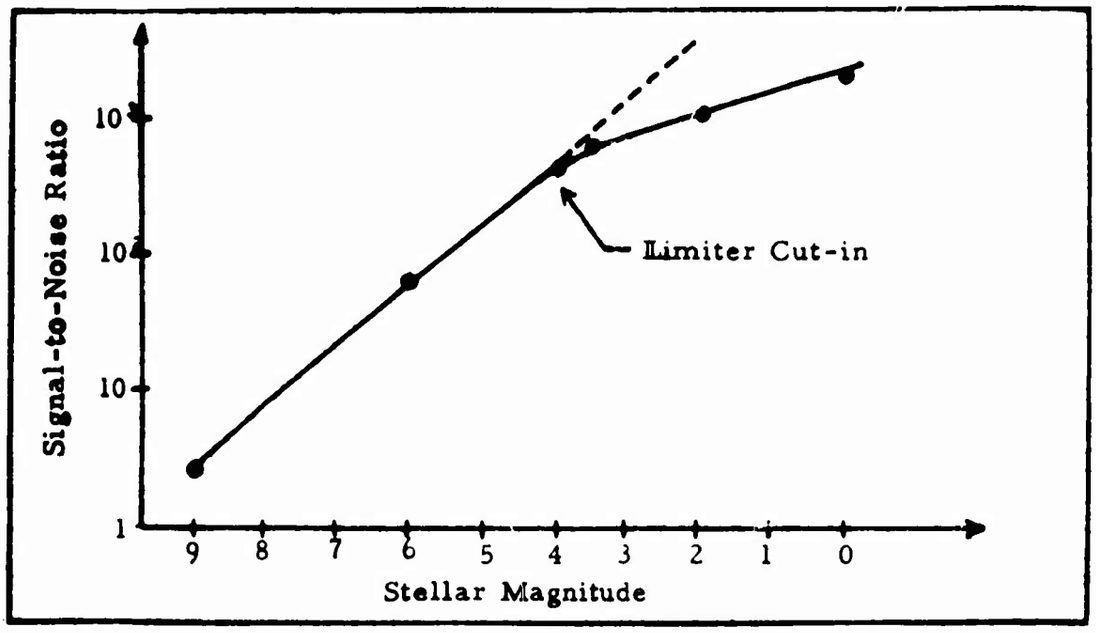

Fig. 19. Signal-to-Noise Ratio as a Function of Stellar Magnitude.

as the maximum E_e for a given stellar magnitude. The dashed portion shows the form of the curve without the limiter functioning. The point of interest is that the S/ N is only slightly more than one for a 9th magnitude target. That means that as the error in position does approach zero, the Error Signal would drop below the noise. A narrow bandwidth would then be required to limit the noise passed on to the servosystem with the Error Signal. The author was concerned with the high noise level encountered. Fig. 20 shows the dark currents for the two PM tubes C11677 and C07182 as functions of dynode voltage, measured to verify that the noise was indeed originating in one of the PM's. The error bars are here used to indicate the range over which the erratic dark current of C11677 fluctuated.

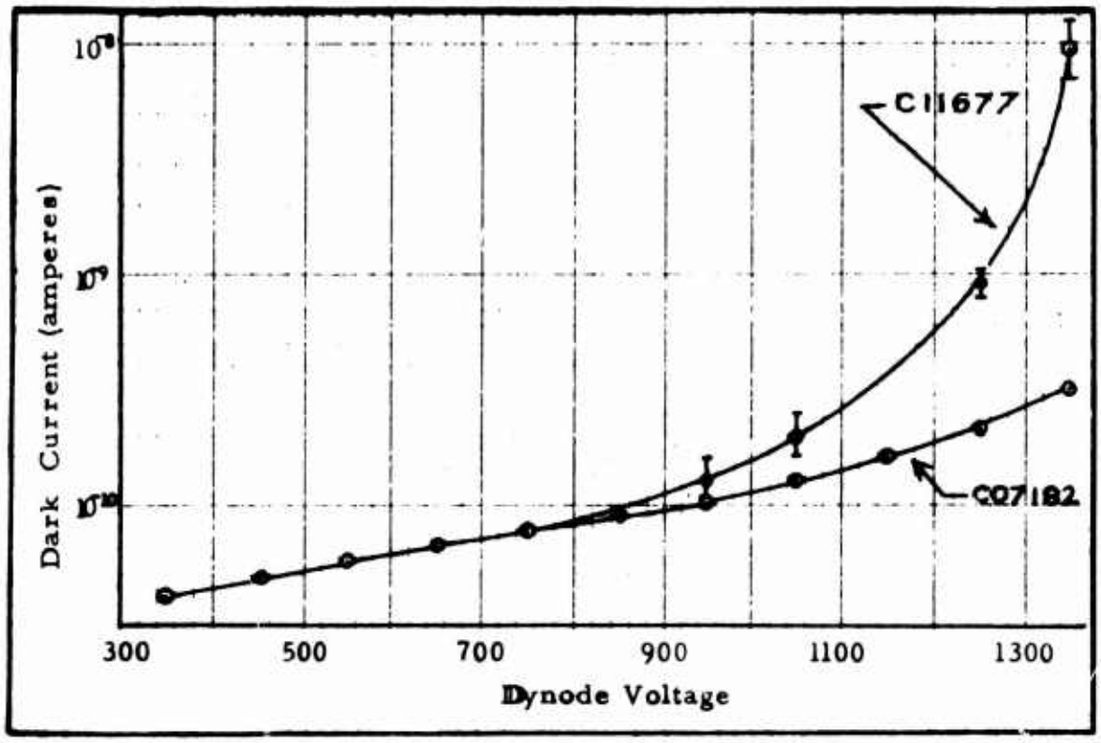

Fig. 20. Dark Current Vs. Dynode Voltage For the Selected PM's.

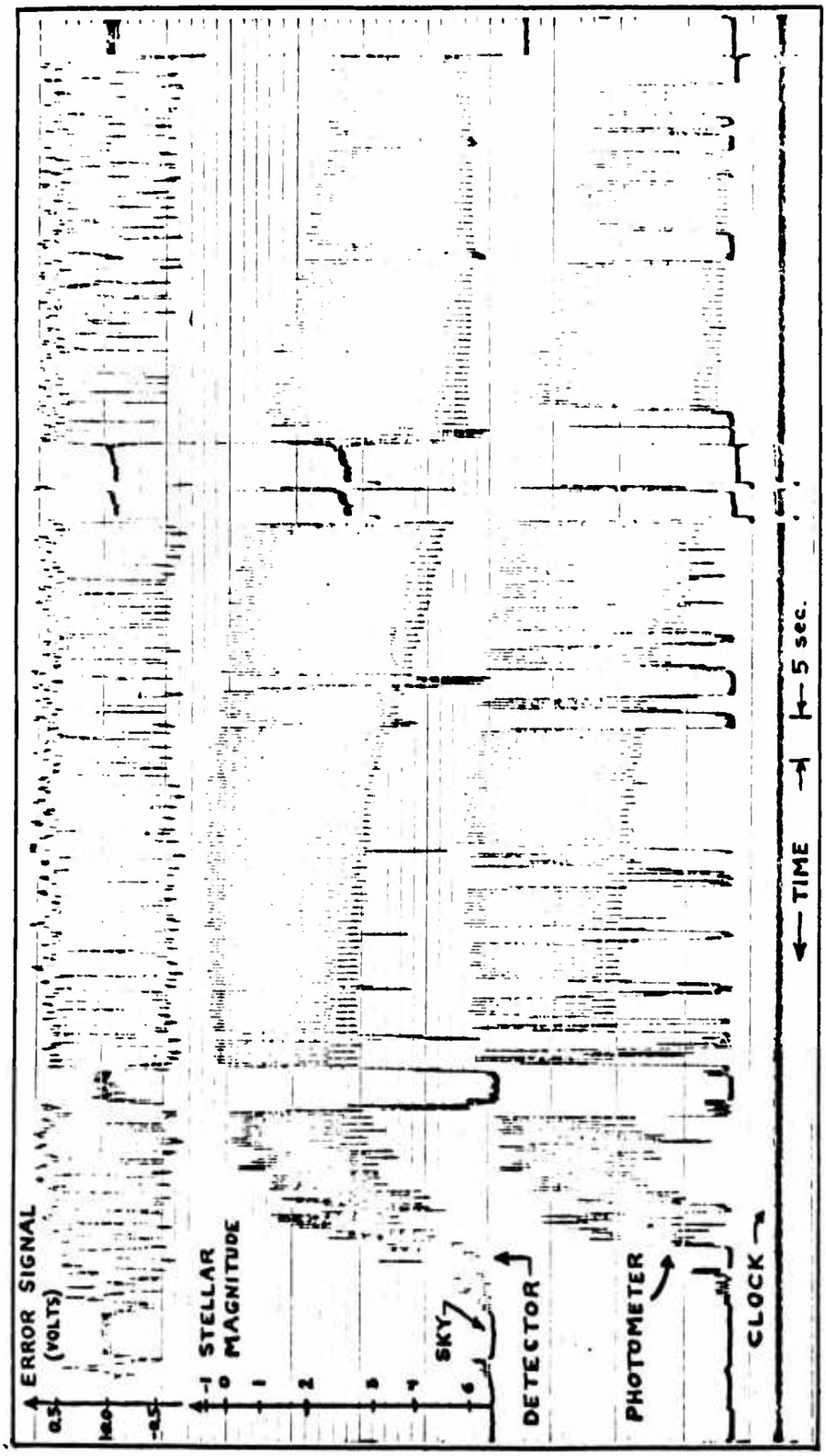

Fig. 21. Transit of Object 3545. 24 NOV 1968 (Intern. Design. 1968 0103B).

The brightest satellite that was tracked was of magnitude -1 at its brightest moment. The target was the rocket body which carried the Russian Proton 4 satellite into orbit. The oscillograph record of that target is shown in Fig. 21. Time increases to the left. The records from top to bottom are the Error Signal fed to the servosystem before processing, target brightness as seen by the detector(Log Output), target brightness as seen by the photometer, and a one pulse per second timing signal from the crystal clock. The photometer's aperture during this transit was 60 arc-seconds. The target was spinning at approximately one cycle per second, resulting in an almost sinusoidal variation in brightness between -1 and 3 stellar magnitudes (stellar magnitude becomes more positive with decreasing brightness). Though it cannot be apparent at this point, the maximum tracking error was less than one image radius. The abrupt drops in brightness down to the sky background level are due to crosstrack errors. The target made this transit under near-perigee conditions (approximately 200 kilometers) and its angular rate exceeded 2° per second. This type of transit is the most difficult for the operator, for tracking errors can accumulate very rapidly. The effectiveness of the detector on this most difficult of targets was limited by the manually applied crosstrack corrections. The long break in the data approximately one-third from the right was due to an inadvertant magnetic tape erasure after the transit was completed. Another example of the operating range of the detector is shown in Fig. 22. The target was the US KAPPA 1 satellite, a modified Agena rocket body, Space Defense Center Catalogue No. 271.

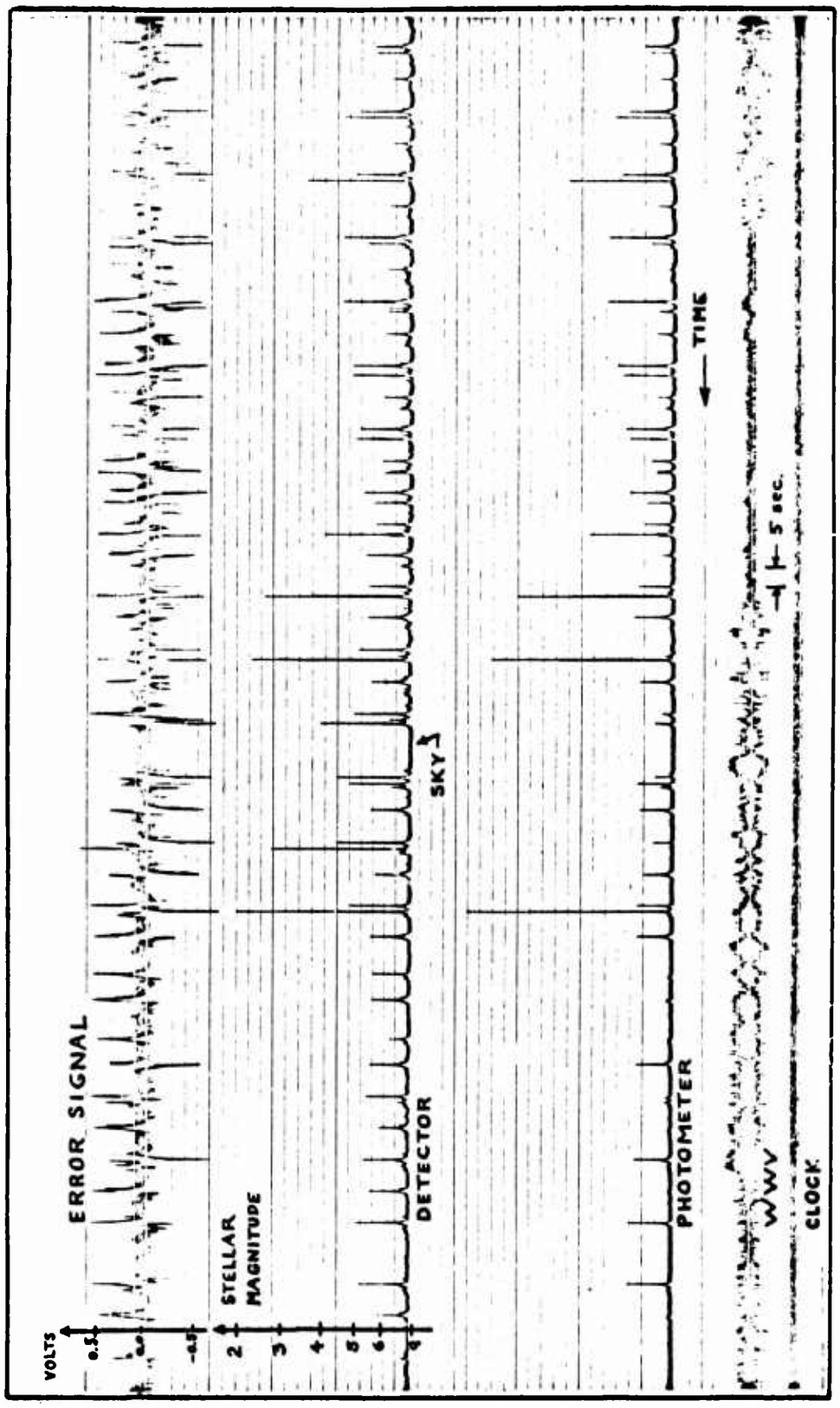

Fig. 22. Transit of Object 271. 24 NOV 1968 (Intern. Design. 62 KAPPA 1).

The records are the same as in Fig. 21 with the addition of a timing signal from WWV, second from the bottom. From the scale of stellar magnitudes one can see that the target had a constant component of brightness of approximately 8.5 magnitude (with excellent, unaided eyesight a 6th magnitude star can be seen). Bright flashes occurring in much less than one second were the result of its spinning. Several flashes reached 2nd magnitude. The polarity of the Error Signal indicates that the detector-telescope combination was randomly hunting on either side of zero error. There is no evidence in this record of an error signal above the noise between flashes, implying one of two things. Either the phase-lag amplifiers removed enough noise to track on the "DC" component of brightness between flashes, or tracking was accomplished on the flashes only. A time expansion of the record revealed that there was a slowly varying component of the error signal between flashes, and the flashes caused only a momentary deviation from zero position error. One would expect that a flash in which the brightness increased by a factor of 400 (largest flash shown) would result in the image being thrown out of the aperture. This did not happen because the limiter held the magnitude (amplitude) of the flash down in the error signal and the reduced transient response prevented the control system from responding catastrophically to the flash. A fixed-gain sensor would not have been able to accept such flashes had it been set to track at the 8.5 magnitude level.

The stellar magnitude scale used on the oscillograph records was obtained by calibrating the Log Output voltage of the detector

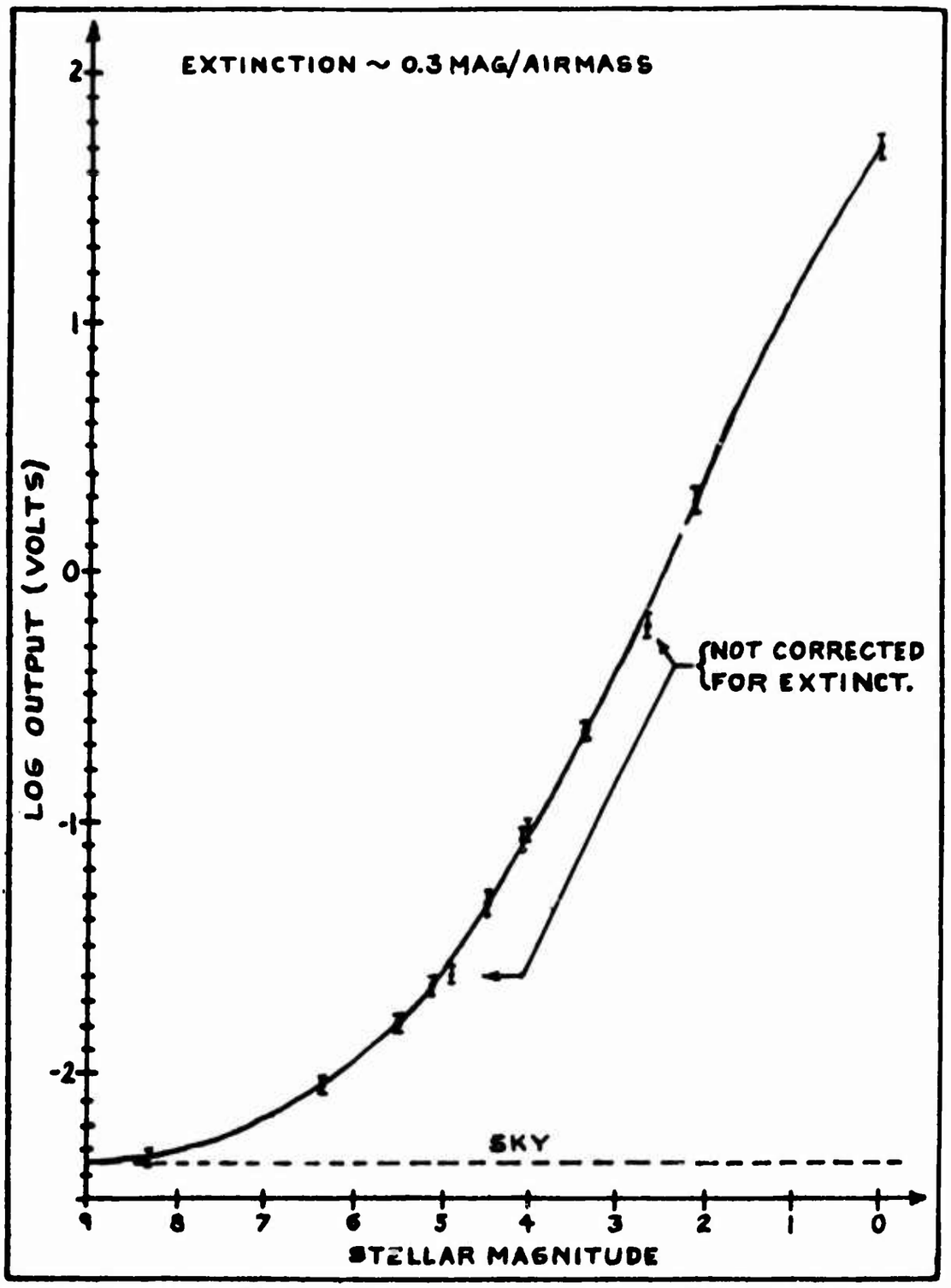

Fig. 23. Calibration Curve of Log Output Voltage Versus Stellar Magnitudes of Class G stars.

against Class G stars of known stellar magnitude. The calibration gave Log Output voltages corresponding to stars of given magnitudes as seen through one airmass (through the zenith) with a certain contribution from the sky background illumination. The method was adopted from the technique used to calibrate the photometer (Ref 9: 79). A typical calibration curve is shown in Fig. 23. Shown on the curve is the error in measuring a given magnitude due to the imbalance in the PM characteristics. The upper limit of error corresponds to the voltage delivered when the star was illuminating only the more sensitive PM; the lower limit is for the opposite case.

The operating range in stellar magnitudes is ultimately defined by the collecting aperture of the telescope with which the detector is coupled. The light gathered by the 24 inch aperture is approximately 1.6×10^{-6} lumens for a -1 magnitude star and 1.6×10^{-10} lumens for a 9th magnitude star (Ref 20: 82). The beam-splitter provided about one-quarter of that light to the detector; by the ratio of areas the effective aperture was therefore only 12 inches. The limiting stellar magnitude of the detector can be found for any aperture by the same method, assuming that the detector threshhold is 4×10^{-11} lumens. For example, with a 10 inch aperture, the detector would be capable of tracking a star of magnitude 8.7 in the limit (with the control system with which it was tested).

Tracking Error. As mentioned before, a great deal of experimenting was required to achieve suitable tracking accuracy. When the

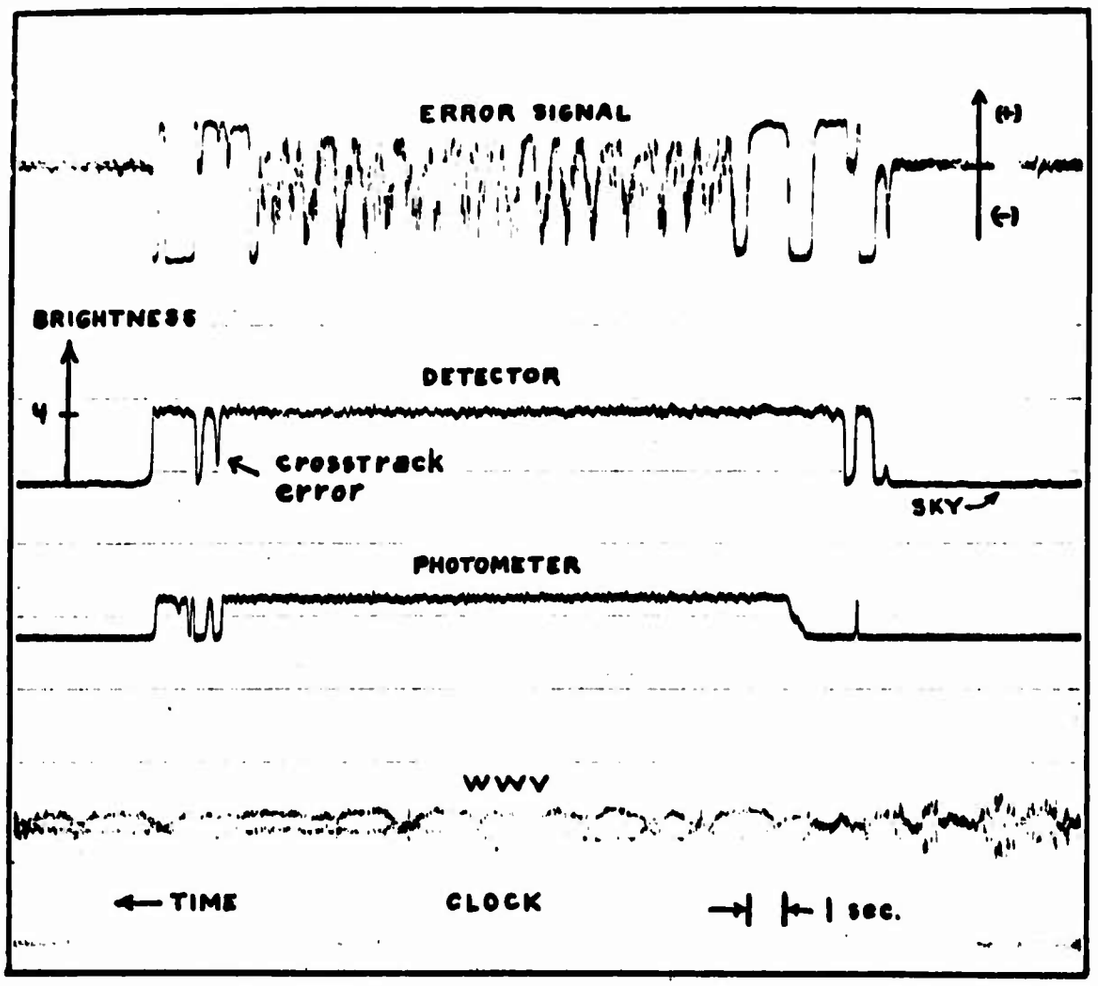

Fig. 24. Record of A Star Being Tracked At Diurnal Rate.

gain was increased to provide good tracking of dim stars, any attempt to track brighter stars resulted in oscillations of the telescope. The author concluded that the description of the servosystem was not complete and the root-locus technique which he used to predict the compensation could not be applied. The root-locus technique consistently predicted an absolutely stable system regardless of the level of the gain. The servosystem itself had been modified during assembly to eliminate instabilities (the author participated in its assembly). Rather than try to develop the required compensation analytically, the author chose

to use trial and error with educated guesses to achieve proper results. Very good results were obtained, as shown in Fig. 24. The record is of a star being tracked and the form of the error signal is of particular interest. The star was allowed to drift into the detector's aperture under diurnal motion. The interpretation of the error signal is that, if E_e at some time is less than the maximum value it can attain with the star, then the position error at that time must be less than one image radius (P less than ±1). It is then apparent that as the star entered the aperture, it first appeared to oscillate slowly from one side to the other before settling down to a random motion about the center of the aperture (of course, the telescope was doing the oscillating). The mean position may not be the center of the aperture if the balance is not perfect, and that situation will be considered in the next section. Similar measurements were made with stars of various stellar magnitudes to determine what variation there might be in the accuracy of tracking. There was no variation in accuracy when a defocused image was used in place of a focused image, so long as the error in position was defined in terms of image radii. There was, however, a definite dependence upon target brightness. The amplitude of the error voltage during the random motion was converted to an amplitude of position error using the curves for error voltage as a function of position error. The change in tracking accuracy (in terms of image radii) with stellar magnitude is shown in Fig. 25. The excursions from zero position error are smallest for targets of about 5th magnitude. The increase in the error for dimmer targets is due to the

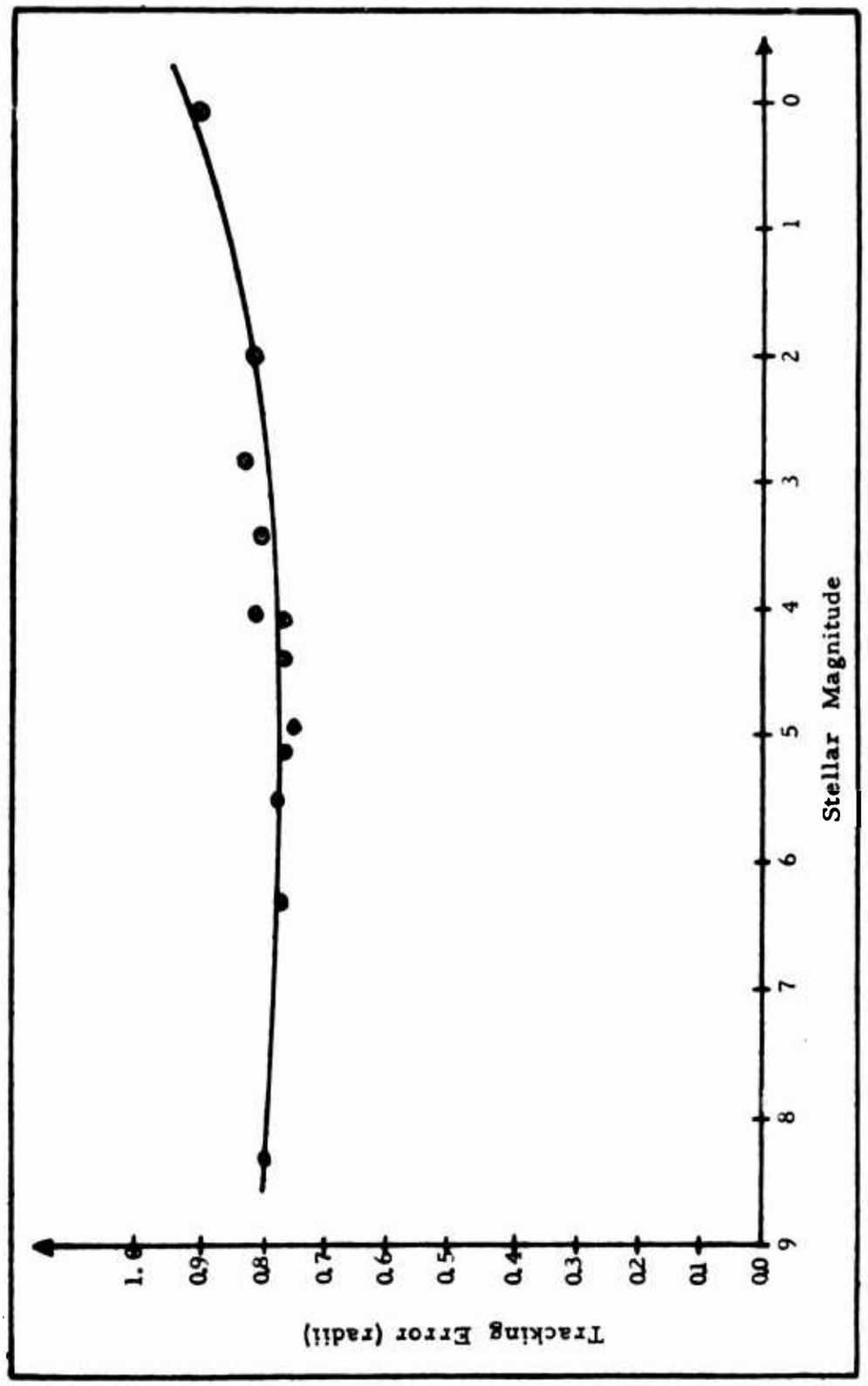

Fig. 25. Tracking Error in Image Radii Versus Stellar Magnitude

decrease in the signal-to-noise ratio. The target must be farther from the center of the aperture to develop an error signal discernible above the noise. At the other end, the error increases due to the increase in the slope of the Error Signal; the closed-loop gain is increased. Under that condition, the system is less stable, rather than more accurate. If the gain were increased sufficiently, oscillations would again set in. The lag compensation effectively moved that required gain high enough so that it was not reached with the brightest target tracked. The tracking accuracy in terms of seconds of arc is dependent upon the size of the image. If 2 seconds of arc is a reasonable size for images of point sources in the ARL telescope, one can conclude that the tracking accuracy was better than ±1 second of arc. In terms of total motion of the image, the wandering in the aperture is less than the diameter, or 2 arc-seconds.

An excellent example of tracking accuracy and of the variation in the Error Signal with target brightness is shown in Fig. 26. The object tracked was the Explorer 19 satellite, a polka-dotted balloon twelve feet in diameter (International Designation 1963 53A). Its slow change in brightness was due to increasing atmospheric extinction as it moved toward the horizon. The slow variation provides a chance to investigate the tracking accuracy as a function of brightness. From the magnitude of the Error Signal when the satellite was first tracked, it is apparent that the tracking error was significantly less than the image radius. One might be tempted to say that the accuracy of tracking increased as the target grew more dim, but it must be remembered that

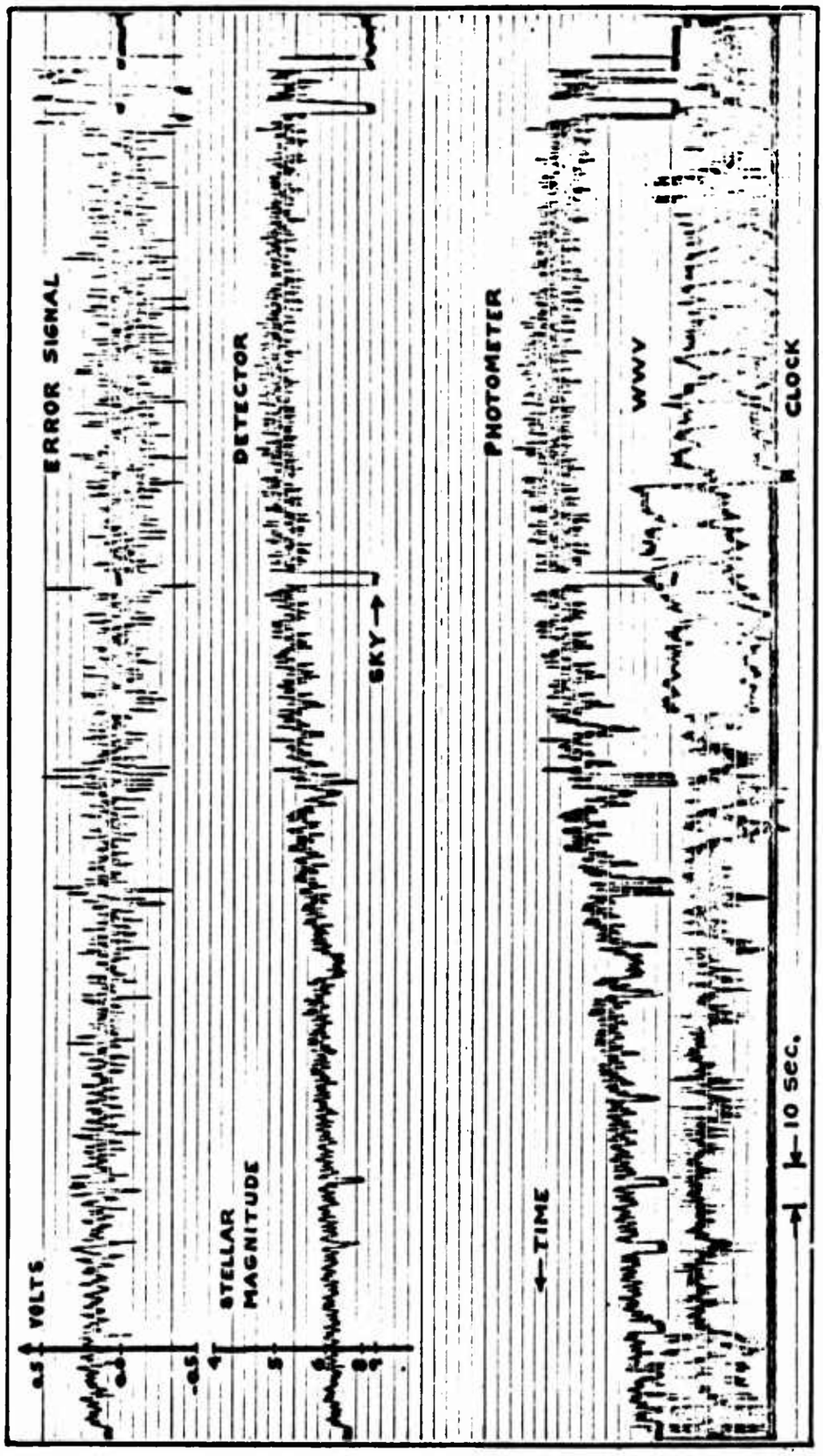

Fig. 26. Transit of Object 714. 4 NOV 1968 (Intern. Design. 1963 53A).

the maximum error signal also decreases. When the target was first acquired, it was near 5th magnitude. so that the tracking accuracy was actually the best at the satellite's brightest moment.

Balance. Measurements of the balance of the detector made with stars brought out an interesting fact. It was that when choosing a pair of photomultiplier tubes one must be careful to match their sensitivities over the spectral range of interest. The tubes chosen for the detector were C11677 and C07182 and their characteristics were best balanced in the laboratory with 80 volts bias applied to the tenth dynode of C07182. When tested on the telescope with stars of the G class, only 22 volts bias was required to achieve the best balance. This indicated that the light source used by the author in the laboratory did not simulate a Class G star, and that the photocathodes of the PM's were more alike than the laboratory tests had shown (for G stars and their spectrum). The same phenomenon was present when C11677 and Z07686 were used together, but Z07686 turned out to be more sensitive to G stars than was C11677. The balance obtainable with these two tubes was decidedly inferior to the balance obtained with the original pair. For that reason, the C11677 was used with the C07182, even though it developed a large dark current.

From Fig. 14, one might predict that the mean position of the image in the detector's aperture need not be the point of zero position error. Fig. 27 shows an example of good tracking of a dim target with bright flashes and a small offset from zero position error. The offset is detectable since more flashes occur with E_e negative than with E_e

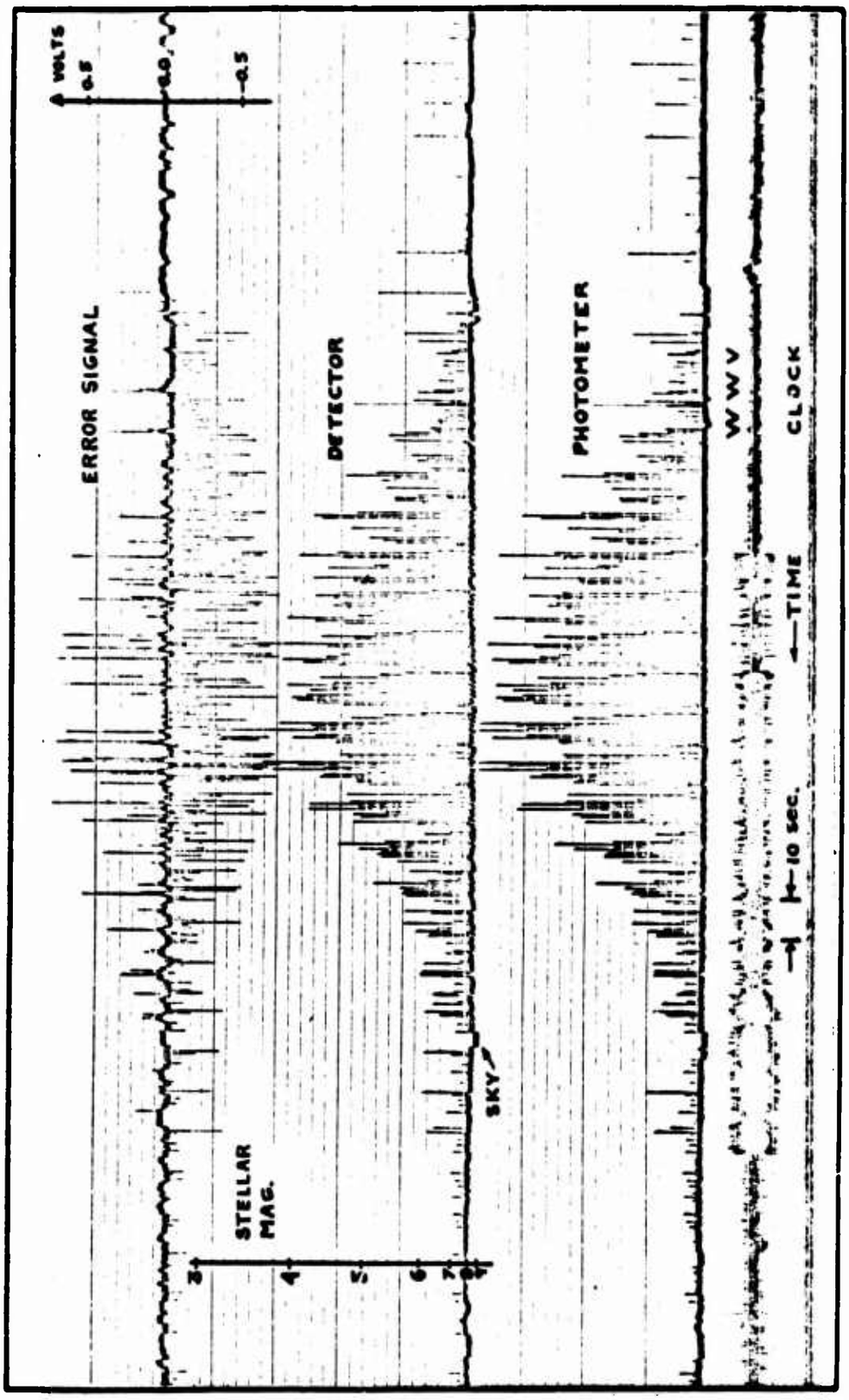

Fig. 27. Transit of Object 2403. 2 NOV 1968 (Intern. Design. 1966 77A).

positive. The target is the US satellite 1966 77A (international designation), Space Defense Center No. 2403. The component of the Error Signal generated by the almost constant 8th magnitude DC component of brightness can be seen underlying the bright flashes.

The effects of detector balance were also analyzed in terms of any modulation they might impart to the brightness of the source as measured at the Log Output. The absence of modulation would allow the detector to be used as a photometer simultaneously with its use as a sensor. The best balance was obtained for targets of magnitude 3.5, but since most satellites change in brightness it was difficult to find a record of a transit which had no modulation on the brightness record. Modulation was determined by comparison to the photometer record which should be a faithful reproduction of the "optical signature" of the satellite. That modulation would be present is certainly to expected in light of the errors noted on the calibration curve of Fig. 23.

Fig. 28 shows a transit with the detector balanced as described. The target is the US 62 B Mu 2 (international designation), Space Defense Center No. 447. Modulation of the detector's brightness record is obvious where the image made definite transits across the edge of the prism. The modulations do not appear on the photometer record, although most of the interesting points were lost due to crosstrack errors. It might be pointed out that the crosstrack errors in part initiated the modulations, for when the image was brought back into the aperture (crosstrack error corrected), it slowly oscillated back and

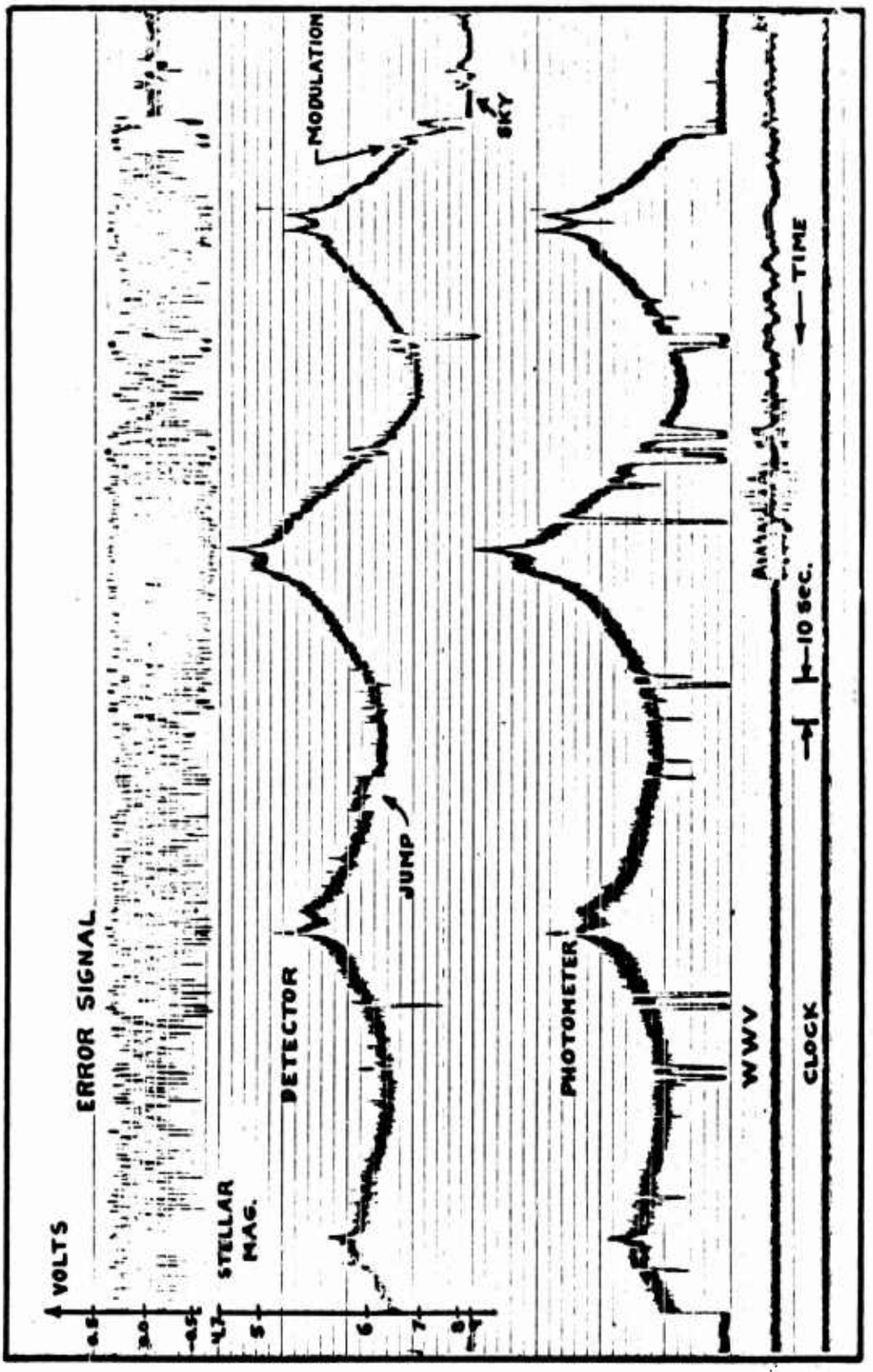

Fig. 28. Transit of Object 447. 24 NOV 1968 (Intern. Design. 62 B Mu 2).

forth across the prism in the characteristic manner of a newly acquired target. The large jump in the detector's brightness record was the result of a shift in the dark current of the PM tube C11677, the "defective" tube. The shift resulted in a temporary imbalance between the two tubes.

The long term stability of the balance was good. On a given night of observation, the balance would return to its preset value (or state) after a warm-up period of approximately 30 minutes. Small drifts were observed during a given night of observation, but they were too small to be detected on the permanent records of data.

Erroneous Target Rejection. One of the most critical problems which can occur with optical trackers is the tendency for the sensor to be attracted to the brightest target in the entrance aperture. The problem is not so severe when tracking slow satellites, but with targets of moderate or high angular rates even a momentary attraction can cause complete loss of tracking. By the time the operator could inhibit the sensor and slew the telescope to continue tracking, the satellite could move into the earth's shadow or pass beyond the horizon. The combination of transient response, diode limiter, and angular rate computer produced an excellent rejection characteristic in the system on the ARL telescope. After the final lag compensation had been installed, locking onto a star never occurred. Of course, the number of times that a very bright star will appear in the small aperture is small, but for many sensors a star of the same brightness as the target can cause confusion. As an example of the rejection characteristic of the detector and servosystem combination, consider Fig. 29. A star of about 4.4

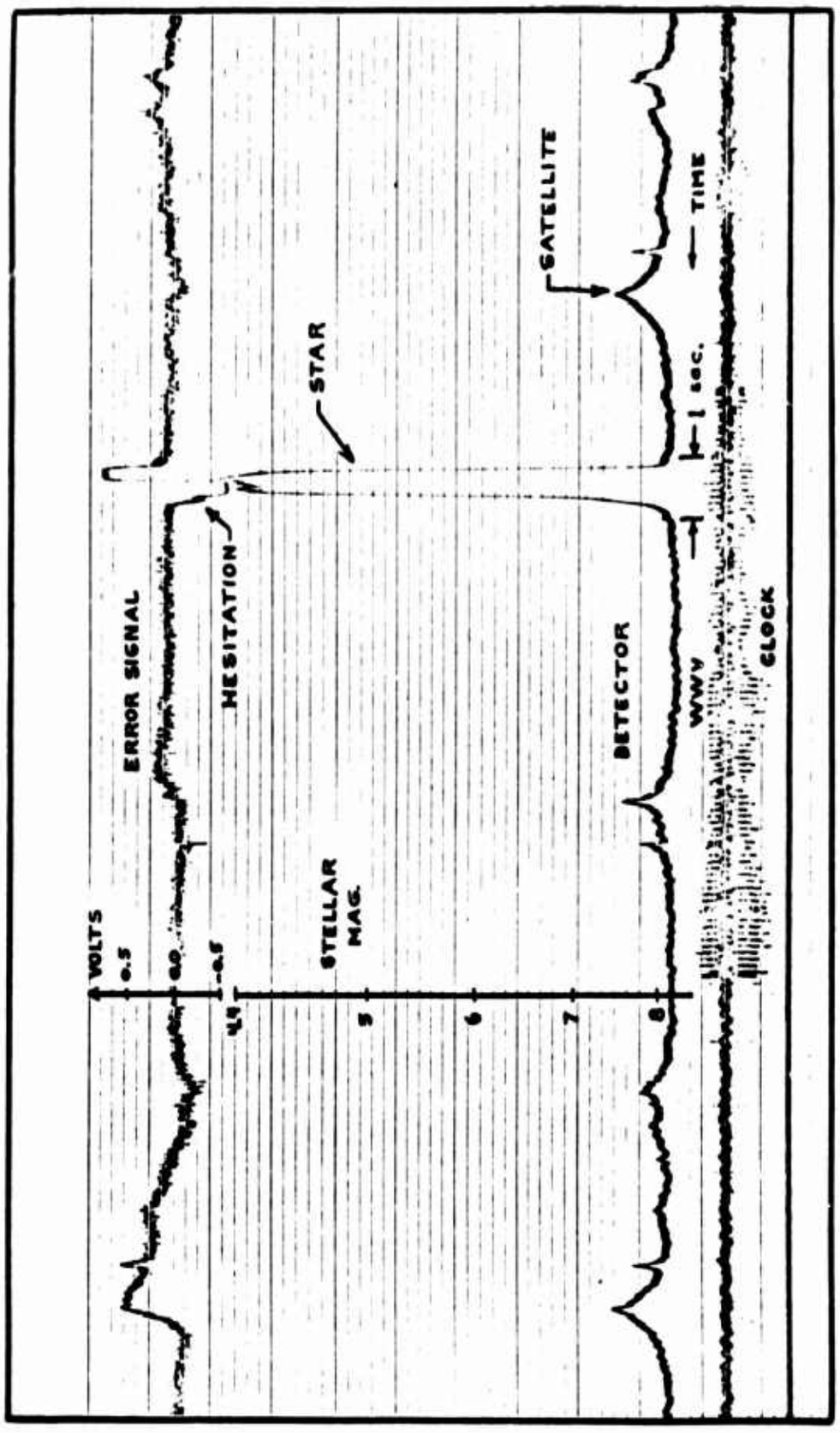

Fig. 29. Transit of 1962 KAPPA 1. 24 NOV 1968. Example of Erroneous Target.

stellar magnitude appeared in the detector aperture while KAPPA 1 was being tracked (as in Fig. 22). The star represented a false target 40 to 50 times brighter than the satellite. Only the slightest hesitation of the telescope is detectable, indicated by the slight flattening of the Error Signal as shown. The detector did not lock onto that star because the maximum amplitude of the Error Signal was not very much greater than the normal error signal from the satellite and the two stages of integral compensation prevented a rapid build-up of the false error signal in the feedback path. In addition, the error signal from the detector is limited to such an extent that the Error Signal never exceeds the output voltage from the analog computer. In the event that an extremely bright star entered the aperture (for example, one of magnitude -1), the detector would certainly attempt to lock onto it. As soon as the detector positioned the telescope on the bright star the Error Signal would be zero, yet the computer would be commanding an angular rate. Thus, the telescope would move off the star and the detector's output would be insufficient to hold it back.

VI. Conclusions

With the evaluation of the device as a position detector and as an optical sensor for satellite tracking completed, the author was able to come to certain conclusions about the prototype. Those conclusions and some recommendations for the improvement of the device or its use will be presented here.

The major consideration in attempting to use two PM tubes in a balanced-bridge configuration lies in selecting a matched pair. The author was very fortunate to have two of three tubes as closely matched as they were. The selection of the matched pair must be carried out with some knowledge of the spectrum of the light source, or better still, some knowledge of the origin of the PM tubes. One is more likely to find a pair of tubes with similar photocathodes and similar electron multipliers within a selection of tubes manufactured at the same time or in the same batch. Once a pair is selected, the simple method of biasing the more sensitive tube is quite effective, yielding the capability of measuring the position of an image to within 0.2 image radii over a brightness range of 10^5. The stability of the detector circuitry was good enough so that, if background illumination is constant and uniform across the entrance aperture, one set of calibration curves for Error Signal versus position error would be reliable for a period of several weeks or more in a laboratory environment.

The evaluation of the detector as a photometer was disappointing, but perhaps not more than could be expected when attempting to

compound the functions of so simple a device. From Fig. 23 one can determine that the uncertainty in measuring the brightness of a target was a function of the brightness. For targets between 0 and 2 stellar magnitudes, the error was ± 0. 1 magnitude. Between 2 and 7 stellar magnitudes, the error decreased to ± 0.05 magnitudes. Below 7th magnitude, the error increased to ± 0.7 magnitudes or more. These numbers were derived from a relatively few number of measurements, but the author feels that the measurement of more stars would only solidify the case against photometry with this detector. The accuracy of the ARL photometer is, at its worst, plus or minus 0.18 stellar magnitudes as determined from almost 2000 measurements. The error in measurement with the detector due to imbalance is in addition to errors inherent in the similar circuitry of the ARL photometer. If one were to become more sophisticated and apply a bias voltage to the more sensitive PM tube in a non-linear fashion to remove all errors in balance, there is a still some doubt that the detector would be usable as a photometer. There is a small but significant loss of light in the image splitter and the noise introduced by the PM tubes is additive. These factors alone would seriously impair the capability to measure small light quantities. It would be extremely difficult to find two low-noise PM tubes which would equal the performance of the PM tube used in the existing ARL photometer. Thus, the author contends that the improvement of the prototype for use as a photometer is not practical.

The operation of the detector as an optical sensor for satellite tracking was quite successful. The tracking accuracy was more than adequate to allow reduction of the ARL photometer's aperture by a

factor of two;several satellites were tracked with the aperture reduced by a factor of four (from 120 arc-seconds to 30 arc-seconds). Above 9th magnitude the tracking accuracy was limited by the crosstrack corrections. For targets around 9th magnitude, the author feels that the observer was applying as much control to the tracking as the detector was. The limiting magnitude was approximately 9th and the brightest target tracked was about -1 magnitude; the dynamic range was therefore 10^4 in brightness. Over that range the error in tracking was less than plus or minus one image radius. Confusion of the sensor by satellites of varying brightness and by stars was a factor which had to be considered when a closed-loop servosystem was proposed (Ref 3:2-4). The automatic gain feature and the erroneous target rejection characteristic of the position detector virtually eliminated all confusion.

On most of the nights of observation, the ARL photometer was sky background limited with a 60 arc-second aperture. It would therefore be desirable to reduce the aperture to 30 arc-seconds to limit the contribution from the sky further. To take full advantage of the detector, the author recommends that the position control on the crosstrack axis be replaced by a velocity control to be corrected occasionally by the detector. Experience has shown that errors in crosstrack occur at a much lower rate than do the track axis errors. The detector could be time-shared between the two axes, perhaps with 90 per cent of the time being spent on the tracking axis. A simple 90 degree image rotator could be used to observe tracking errors in two dimensions. With automatic control on both axes, a 30 arc-second aperture on the photometer would be quite practical.

To improve on the prototype, the author would make several

changes. The aperture on the detector was made large for test purposes and was shown to be in excess. A smaller aperture would reduce the background illumination and improve dim target detection. The dual voltage-divider resistances could be replaced by a single unit to reduce the chance of a component value change effecting only one PM. Low-noise operational amplifiers of solid-state construction and with high input impedances could be mounted on the detector head to replace the cathode-followers. These changes would reduce the heating in the head and lower the thermionic dark current in the PM tubes. The best results can be obtained with a new matched pair of photomultiplier tubes. Low-noise, high sensitivity PM tubes, coupled with a reduced aperture, could significantly improve the dim target detection.

The four basic requirements for a desirable satellite tracking detector were met with the prototype device. The performance of the detector was so satisfactory that it was put into regular use on those targets which exceed its sensing threshhold brightness.

Bibliography

1. Baker, R.H. Astronomy (Seventh Edition). Princeton: D. Van Nostrand Co., 1961.

2. Burr-Brown Research Corp. Handbook of Operational Amplifier Applications. Tucson: Burr-Brown Research Corp., 1963.

3. Douglas Report SM-52046P. Proposal to Perform A Satellite Tracker Servo-System Study. Santa Monica, Calif.: Missle and Space Systems Division of Douglas Aircraft Co., Inc., April 1966.

4. Engstrom, R.W. "Multiplier Photo-tube Characteristics: Application to Low Light Levels." Journal of the Optical Society of America, 37 : 420-431 (June 1947).

5. Engstrom, R.W. and E. Fischer. "Effects of Voltage-Divider Characteristics On Multiplier Phototube Response." The Review of Scientific Instruments , 28: 525-527 (July, 1957).

6. Hariharan, P. and M.S. Bhalla. "Linear Photomultiplier Bridge Circuit for the Measurement of Small Changes in Absorption." British Journal of Applied Physics , 10: 89-90 (February, 1959).

7. Jenkins, F.A. and H.E. White. Fundamentals of Optics (Third Edition). New York: McGraw-Hill, 1957.

8. Kennedy, H.B. Satellite Tracker Servo System Design. Redondo Beach, Calif.: Logicon, Inc., April 1967.

9. Kissell, K.E. "Photoelectric Photometry-A New Tool for Satellite Signatures." Proceedings of the OAR Research Applications Conference : 71-99 (April 1966).

10. Lago, G. and L.M. Benningfield. Control System Theory . New York: Ronald Press, 1962.

11. Larsen, C.C. and H.S. Salinger. " Photo-Cell Multiplier Tubes." The Review of Scientific Instruments , 11 : 226-229 (July 1940).

12. Millman, J. Vacuum-tube and Semiconductor Electronics . New York: McGraw-Hill, 1958.

13. Pearson, E.B. Technology of Instrumentation. Princeton: D. Van Nostrand, 1957.

14. RCA Electron Tube Division. 7029 Multiplier Photo-Tube. Tentative Data. Harrison, N.J.: RCA, December 1957.

15. Rome, M., et al. "The Quadrant Multiplier Phototube, A New Star-Tracker Sensor." Applied Optics , 3 : 691-695 (June 1964).

16. Schwartz, M. Information Transmission, Modulation, And Noise. New York: McGraw-Hill, 1959.

17. Seely, S. Electronic Circuits. New York: Holt, Rinehart, and Winston, 1968.

18. Sweet, M.H. "An Improved Photomultiplier Tube Color Densitometer." Journal of the SMPTE, 54 : 35-62 (January 1950).

19. Vanderburgh, R.C. Photoelectric Measurements of Optical Glints From Orbiting Spacecraft. Presented to the 1968 Science and Engineering Symposium, USAF Academy, October 30-November 1, 1968. Wright-Patterson Air Force Base, Ohio:General Physics Laboratory of ARL.

20. Whitford, A. and E. Kron. "Photoelectric Guiding of Astronomical Telescopes." The Review of Scientific Instruments , 8:71-74 (March 1937).

VITA

Louis Stephen Macknik [redacted]

He graduated from high school in Bridgeton, N. J. in 1960 and attended Drexel Institute of Technology until he enlisted in the USAF in 1964. After Basic Training, he attended the Ground Radio Equipment Repairman School at Keesler AFB, Miss., completing the course in April, 1965. Under the Airman Education and Commissioning Program, he entered the University of Missouri at Columbia, Mo., in June, 1965. He was elected to Eta Kappa Nu and Tau Beta Pi and received the degree of Bachelor of Science in Electrical Engineering in January, 1967. He attended Officer Training School and was commissioned in the USAF in April, 1967.

[redacted]

Unclassified
Security Classification

DOCUMENT CONTROL DATA - R & D

(Security classification of title, body of abstract and indexing annotation must be entered when the overall report is classified)

1. ORIGINATING ACTIVITY *(Corporate author)* Air Force Institute of Technology (AFIT-SE) Wright-Patterson AFB, Ohio 45433	2a. REPORT SECURITY CLASSIFICATION Unclassified 2b. GROUP

3. REPORT TITLE

A Photoelectric Position Detector For Satellite Tracking

4. DESCRIPTIVE NOTES *(Type of report and inclusive dates)*

AFIT Thesis

5. AUTHOR(S) *(First name, middle initial, last name)*

Louis S. Macknik
1/ Lt USAF

6. REPORT DATE	7a. TOTAL NO. OF PAGES	7b. NO. OF REFS
February 1969	76	20

8a. CONTRACT OR GRANT NO. b. PROJECT NO. N/ A c. d.	9a. ORIGINATOR'S REPORT NUMBER(S) GSP/ PH/ 69-11 9b. OTHER REPORT NO(S) *(Any other numbers that may be assigned this report)*

10. DISTRIBUTION STATEMENT This document is subject to special export controls and each transmittal to foreign governments or foreign nationals may be made only with prior approval of the Dean of Engineering Air Force Institute of Technology (AFIT-SE), Wright-Patterson Air Force Base, Ohio 45433.

11. SUPPLEMENTARY NOTES	12. SPONSORING MILITARY ACTIVITY

13. ABSTRACT

A photoelectric position detector consisting of two photomultiplier tubes, an image splitter, and associated electronics was constructed. Negative feedback was used for automatic gain control of the multiplier tubes in a bridge circuit. The output currents of the multiplier tubes were compared to detect image position to within 0.2 image radii. With a satellite tracker servosystem, artificial satellites were tracked to within one arc-second over a brightness range of ten thousand. Detection threshhold was 4×10^{-11} lumens. Bridge imbalance negated the detector's use as a photometer.

DD FORM 1 NOV 65 1473

Unclassified
Security Classification

14. KEY WORDS	LINK A		LINK B		LINK C	
	ROLE	WT	ROLE	WT	ROLE	WT
Photoelectric satellite tracker						
Photomultiplier						
Satellite tracking						
Logarithmic response satellite tracker						
Optical Satellite tracking						